Propene Pyrolysis and Oxidation Kinetics in a Flow Reactor and Laminar Flames

S. G. DAVIS[†] **and C. K. LAW**
Department of Mechanical and Aerospace Engineering, Princeton University, Princeton, NJ 08544

and

H. WANG*
Department of Mechanical Engineering, University of Delaware, Newark, DE 19716

The pyrolysis and oxidation of propene were studied experimentally in an atmospheric flow reactor. Species profiles were obtained in the intermediate to high temperature range (~1200 K) for lean, stoichiometric, rich, and pyrolytic conditions. Laminar flame speeds of propene/air mixtures were also determined over an extensive range of equivalence ratios, at room temperature and atmospheric pressure, using the counterflow twin flame configuration. A detailed chemical kinetic model consisting of 469 reactions and 71 species was used to describe the high-temperature kinetics of propene, propyne, allene, and propane. It was shown that the kinetic model could accurately predict a wide range of combustion data for these fuels, including laminar premixed flame speeds, speciation in flow reactors, and ignition in shock tubes. Notable uncertainties in the reaction kinetics of these fuels are identified and discussed.

INTRODUCTION

Propene (C_3H_6) is a key intermediate in the combustion of higher alkanes, such as propane, butane, heptane, and iso-octane [1–3]. These hydrocarbon compounds constitute a notable part of practical hydrocarbon fuels. Understanding the chemical kinetic submechanism for the pyrolysis and oxidation of propene is essential for determining the overall kinetic mechanism of larger fuels. Furthermore, the high-temperature kinetics of propene pyrolysis and oxidation are relevant to the formation of aromatics, possibly via allene, propyne, and the propargyl radical [4–6].

Various studies have examined propene oxidation at high temperatures. Propene/air flame speeds were measured by Gibbs and Calcote [7], Gerstein et al. [8], and Günther and Janisch [9], although the accuracy of these data was complicated by the effect of flame stretch coupled with mixture nonequidiffusion, and by nonadiabaticity [3]. The oxidation of propene behind reflected shock waves was examined by Burcat and Radhakrishnan [10]. In that study, the ignition delay times were measured for temperatures in the range of 1274–1840 K and for pressures between 2–7 atm; and product distributions were reported and compared with predictions using the detailed kinetic model of Westbrook and Pitz [11]. Comparisons between experimental data and modeling results showed that only partial agreement was achieved, rendering the established kinetic pathways of propene ignition inconclusive [10]. Dagaut et al. [12, 13] studied the high-temperature oxidation of propene in laminar premixed flames and in a jet-stirred reactor (JSR) for temperatures ranging from 900–1200 K, pressures in the range of 1–8 atm, and for mixture equivalence ratios ranging from 0.15 to 4.0. Their kinetic model predicted relatively well the major species profiles experimentally determined in the JSR. Fair agreement was obtained in their predictions of the laminar flame speed data of Refs. 7 and 9. Using molecular-beam mass spectrometry, Thomas [14] recently determined the profiles of stable species and free radicals in a lean (ϕ = 0.229), low-pressure (p = 30 Torr) laminar premixed propene–oxygen–argon flame. A subsequent modeling study by Thomas et al. [15] showed that the major species profiles could be

[†]Present address: IRPHE—Laboratoire de Combustion, Service 252, Faculté de St. Jérôme, 13397 Marseille Cedex 20, France.
*Corresponding author. E-mail: hwang@me.udel.edu, davis@lrc.univ-mrs.fr

COMBUSTION AND FLAME 119:375–399 (1999)

Published by Elsevier Science Inc.
0010-2180/99/$–see front matter
PII S0010-2180(99)00070-X

well reproduced by the proposed kinetic model, and that propene was mainly consumed by its reaction with the O-atom leading to C_1 and C_2 fragments. At the same time, they identified the need for more experimental and theoretical work on the rates and product distribution of the attack of O and OH on propene, and for the allyl (aC_3H_5) + O_2 reactions.

There have been a number of experimental and computational studies on propene oxidation at low and intermediate temperatures in stirred reactors, as reviewed by Wilk et al. [16]. They also examined the oxidation of propene in a stirred reactor at temperatures between 530 and 740 K, equivalence ratios of 0.8–2.0, and at 600 Torr. At these conditions, a regime of negative temperature coefficient behavior was observed experimentally and predicted by the model, and the intermediate product distributions were found to be very sensitive to the addition and abstraction reactions of OH and propene. The concentration profiles of acetaldehyde and CO were reproduced well; however, prediction of other species profiles were met with mixed results. Recently, Stark and Waddington [17] studied the oxidation of propene under fuel-rich conditions in the temperature and pressure range of 505–549 K and 0.9–4 atm, respectively. Under these conditions, oxygenated species were prevalent with propene oxide being the dominate product followed by formaldehyde and acetaldehyde.

A number of studies on propene pyrolysis [18–21] were reviewed by Hidaka et al. [22], who also studied the thermal decomposition of propene behind reflected shock waves at temperatures between 1200–1800 K and molar densities between 1.6–2.7 $\times 10^{-5}$ mol/cm^3, using IR laser absorption spectroscopy and gas chromatography. The study showed that the major pyrolysis products were ethylene, methane, and acetylene, and that propyne concentrations were larger than those of allene throughout the entire experimental domain. Hidaka et al. [22] also showed that there were considerable discrepancies in the reported rates of propene C-H and C-C fission reactions

$$C_3H_6 = aC_3H_5 + H \qquad (-R1)$$

$$C_3H_6 = C_2H_3 + CH_3, \qquad (-R2)$$

the only two reaction channels previously considered for the initiation process. They found that existing shock-tube data could not be reconciled by just these two initiation reactions. On the basis of thermochemical considerations, they proposed that an additional reaction step,

$$C_3H_6 = C_2H_2 + CH_4$$

must be included to obtain reasonable agreement between experiment and modeling. The newly proposed reaction originates from the consideration that vinylidene can insert into the C-H bond of CH_4 in the reverse direction. It was proposed that the latter reaction has an activation energy of 73.8 kcal/mol, which is lower than those of the direct C-H and C-C fission reactions by 13 and 24 kcal/mol, respectively.

In pursuing a converged kinetic mechanism of C_3H_x combustion, we recently undertook a series of studies which examined the kinetics of propyne and allene pyrolysis and oxidation experimentally, computationally, and theoretically [23, 24]. An experimental and modeling study of propyne pyrolysis in a flow reactor and a kinetic modeling of both propyne and allene pyrolysis in shock tubes were reported [24]. In the present work, we extend this study to propene pyrolysis and oxidation. Specifically, the laminar flame speeds of propene/air mixtures were determined over an extensive range of equivalence ratios (ϕ = 0.7 to 1.7) and at atmospheric pressure. In addition, propene pyrolysis and oxidation (ϕ = 0.7, 1.0, 1.4) were experimentally studied at temperatures around 1200 K using the Princeton Turbulent Flow Reactor (PTFR). These experimental works constitute the first objective of the study.

The second objective is to perform detailed kinetic modeling with the aim of reconciling propene kinetics over a wide range of conditions, and ultimately reconciling the kinetics of all C_3H_x fuels in general. For this purpose, we also present and discuss the modeling results of propyne oxidation in the PTFR, laminar premixed flames, allene and propyne oxidation in shock tubes, and of propane oxidation in laminar premixed flames and shock tubes. The remaining uncertainties in the kinetics of propene and propyne are identified and discussed.

EXPERIMENTAL METHODOLOGIES

The counterflow twin flame technique [25] was used to determine the laminar flame speed, with both linear [26] and nonlinear extrapolations [27]. Details of the technique can be found in Refs. 25–27. It is worth noting that the accuracy of the present extrapolation is adequate in that the Karlovitz number was maintained below 0.1. A Hastings mass flow controller was used to meter the propene flow rate, while the remaining gases (O_2, N_2, and air) were metered by sonic orifices. A TSI argon-ion laser Doppler velocimetry system (496 nm) was used to measure the axial flow velocity. All experiments were conducted at atmospheric pressure and at equivalence ratios ranging from 0.7 to 1.7, using propene with a purity $\geq$99.5%.

Specifications of the PTFR have been documented elsewhere [28]. In the experimentation the gas samples were collected in a water-cooled sampling probe and analyzed using a 5890 Hewlett-Packard gas chromatograph with a flame ionization detector (FID). CO, CO_2, and C_1–C_4 hydrocarbon species were eluted from a PlotQ column, while C_5 and higher hydrocarbons were eluted from a DB-5 column. Species were identified by retention time matching. FID signals of the product yields were quantified and converted into mole fractions using extensive calibrations from a gravimetrically blended, certified gas mixture, with the exception of cyclopentadiene, vinylacetylene, and an unidentified oxygenated species to be discussed later. Carbon balances were carefully checked for all conditions and found to be within 6% of the mean value. All experiments were conducted at atmospheric pressure and with nitrogen as the diluent. Conversion of flow reactor data from a spatial frame to a temporal frame was accomplished by assuming plug flow conditions throughout most of the reactor, except in the early stages where an effective area formulation, based on experimental flow field measurements, was used.

The initial mixture composition and temperature for the pyrolysis and oxidation experiments are given in Table 1. The mixtures used in the oxidation study ranged from fuel-lean to fuel-rich conditions, with equivalence ratios of 0.7, 1.0, and 1.4. For all mixtures, the initial temperature was about 1200 K to ensure ample fuel decomposition within the allowable reaction time in the PTFR.

TABLE 1

Initial Conditions for Propene Pyrolysis and Oxidation in the PTFR

	Mole Fraction			
ϕ	C_3H_6	O_2	N_2	T_o(K)
∞	0.00288	0.00000	0.99712	1210
0.7	0.00303	0.01948	0.97749	1170
1.0	0.00296	0.01330	0.98374	1181
1.4	0.00291	0.00924	0.98785	1200

KINETIC MODEL SPECIFICATION

The detailed kinetic model contains 71 species and 469 reactions. The kinetics for the C_1 and C_2 species are based on the GRI-Mech 1.2 [29], which was further expanded and validated against fundamental combustion data including the laminar flame speeds of methane [29, 30], ethylene, and acetylene [31], species profiles in laminar premixed flat flames [32] and in counterflow diffusion flames of acetylene and ethylene [31]. The reactions which extend the model beyond GRI-Mech 1.2 are shown in Table 2. In what follows, we shall discuss several important features of this kinetic model.

Substantial modifications and additions to the kinetics of propyne (pC_3H_4), allene (aC_3H_4), propargyl (C_3H_3), allyl (aC_3H_5), and CH_3CCH_2 were made in our recent studies [23, 24] of the oxidation and pyrolysis of propyne and allene. The specific reaction rate coefficients closely examined include: (a) the mutual isomerization of allene and propyne via cyclopropene as a vibrationally excited state as well as a stabilized intermediate,

$$aC_3H_4 \leftrightarrow cC_3H_4 \leftrightarrow pC_3H_4,$$

(b) the chemically activated and unimolecular reactions on the C_3H_5 potential energy surface, including but not limited to

$$aC_3H_5 \rightarrow aC_3H_4 + H \qquad (-R50)$$

$$pC_3H_4 + H \rightarrow aC_3H_4 + H \qquad (-R48)$$

$$pC_3H_4 + H \rightarrow C_2H_2 + CH_3. \qquad (-R46)$$

TABLE 2

Detailed Kinetic Model[a]

No.	Reaction[b]	$k = AT^n \exp(-E/RT)^c$ A	n	E	References/Comments
	Reactions of propene				
1	$aC_3H_5 + H(+M) = C_3H_6(+M)$	2.00×10^{14}			k_∞, *d*
		1.33×10^{60}	−12.0	5,968	k_0
	$a = 0.020$	$T^{***} = 1{,}097$	$T^* = 1{,}097$	$T^{**} = 6{,}860$	*e*
2	$CH_3 + C_2H_3(+M) = C_3H_6(+M)$	2.50×10^{13}			k_∞, *f*
		4.27×10^{58}	−11.94	9,770	k_0
	$a = 0.175$	$T^{***} = 1{,}341$	$T^* = 60{,}000$	$T^{**} = 10{,}140$	*e*
3	$C_3H_6 + H = C_2H_4 + CH_3$	1.60×10^{22}	−2.39	11,180	1 atm, *g*
4	$C_3H_6 + H = aC_3H_5 + H_2$	1.70×10^{05}	2.5	2,490	[33]
5	$C_3H_6 + H = CH_3CCH_2 + H_2$	4.00×10^{05}	2.5	9,790	[33]
6	$C_3H_6 + O = CH_2CO + CH_3 + H$	1.20×10^{08}	1.65	327	[33]
7	$C_3H_6 + O = C_2H_5 + HCO$	3.50×10^{07}	1.65	−972	[33]
8	$C_3H_6 + O = aC_3H_5 + OH$	1.80×10^{11}	0.7	5,880	[33]
9	$C_3H_6 + O = CH_3CCH_2 + OH$	6.00×10^{10}	0.7	7,630	[33]
10	$C_3H_6 + OH = aC_3H_5 + H_2O$	3.10×10^{06}	2.0	−298	[33]
11	$C_3H_6 + OH = CH_3CCH_2 + H_2O$	1.10×10^{06}	2.0	1,450	[33]
12	$C_3H_6 + HO_2 = aC_3H_5 + H_2O_2$	9.60×10^{03}	2.6	13,910	[33]
13	$C_3H_6 + CH_3 = aC_3H_5 + CH_4$	2.20×10^{00}	3.5	5,675	[33]
14	$C_3H_6 + CH_3 = CH_3CCH_2 + CH_4$	8.40×10^{-01}	3.5	11,660	[33]
	Reactions of allyl				
15	$CH_3 + C_2H_2 = aC_3H_5$	2.68×10^{53}	−12.82	35,730	1 atm, [24]
16	$CH_3 + C_2H_3 = aC_3H_5 + H$	1.50×10^{24}	−2.83	18,618	1 atm, *f*
17	$aC_3H_5 + H = aC_3H_4 + H_2$	1.80×10^{13}			[33]
18	$aC_3H_5 + O = C_2H_3CHO + H$	6.00×10^{13}			[33]
19	$aC_3H_5 + OH = C_2H_3CHO + H + H$	4.20×10^{32}	−5.16	30,126	1 atm, [33]
20	$aC_3H_5 + OH = aC_3H_4 + H_2O$	6.00×10^{12}			[33]
21	$aC_3H_5 + O_2 = aC_3H_4 + HO_2$	4.99×10^{15}	−1.4	22,428	[36]
22	$aC_3H_5 + O_2 = CH_3CO + CH_2O$	1.19×10^{15}	−1.01	20,128	[36]
23	$aC_3H_5 + O_2 = C_2H_3CHO + OH$	1.82×10^{13}	−0.41	22,859	[36]
24	$aC_3H_5 + HO_2 = C_3H_6 + O_2$	2.66×10^{12}			[37]
25	$aC_3H_5 + HO_2 = OH + C_2H_3 + CH_2O$	6.60×10^{12}			[37]
26	$aC_3H_5 + HCO = C_3H_6 + CO$	6.00×10^{13}			[33]
27	$aC_3H_5 + CH_3 = aC_3H_4 + CH_4$	3.00×10^{12}	−0.32	−131	[33]
28	$aC_3H_5 = CH_3CCH_2$	7.06×10^{56}	−14.08	75,868	1 atm, [24]
	Reactions of CH_3CCH_2				
29	$CH_3 + C_2H_2 = CH_3CCH_2$	4.99×10^{22}	−4.39	18,850	1 atm, [24]
30	$CH_3CCH_2 + H = pC_3H_4 + H_2$	3.34×10^{12}			estimated
31	$CH_3CCH_2 + O = CH_3 + CH_2CO$	6.00×10^{13}			estimated
32	$CH_3CCH_2 + OH = CH_3 + CH_2CO + H$	5.00×10^{12}			estimated
33	$CH_3CCH_2 + O_2 = CH_3CO + CH_2O$	1.00×10^{11}			estimated
34	$CH_3CCH_2 + HO_2 = CH_3 + CH_2CO + OH$	2.00×10^{13}			estimated
35	$CH_3CCH_2 + HCO = C_3H_6 + CO$	9.00×10^{13}			estimated
36	$CH_3CCH_2 + CH_3 = pC_3H_4 + CH_4$	1.00×10^{11}			estimated
	Reactions of C_2H_3CHO				
37	$C_2H_3 + HCO = C_2H_3CHO$	1.80×10^{13}			k_∞, [33]
38	$C_2H_3CHO + H = C_2H_4 + HCO$	1.08×10^{12}	0.45	1,820	estimated
39	$C_2H_3CHO + O = C_2H_3 + OH + CO$	3.00×10^{13}		3,540	estimated
40	$C_2H_3CHO + O = CH_2O + CH_2CO$	1.90×10^{07}	1.8	220	estimated
41	$C_2H_3CHO + OH = C_2H_3 + H_2O + CO$	3.43×10^{09}	1.18	−447	estimated

(continued on next page)

TABLE 2, Continued

No.	Reaction[b]	$k = AT^n \exp(-E/RT)$[c] A	n	E	References/Comments
	Reactions of propyne and allene				
42	$pC_3H_4 = cC_3H_4$	1.20×10^{44}	−9.92	69,250	1 atm, [24]
43	$pC_3H_4 = aC_3H_4$	5.15×10^{60}	−13.93	91,117	1 atm, [24]
44	$cC_3H_4 = aC_3H_4$	4.89×10^{41}	−9.17	49,594	1 atm, [24]
45	$C_3H_3 + H = pC_3H_4$	1.50×10^{13}			see text
46	$CH_3 + C_2H_2 = pC_3H_4 + H$	2.56×10^{09}	1.1	13,644	1 atm, [24]
47	$pC_3H_4 + H = C_3H_3 + H_2$	1.30×10^{06}	2.0	5,500	*h*
48	$pC_3H_4 + H = aC_3H_4 + H$	6.27×10^{17}	−0.91	10,079	1 atm, [24]
49	$pC_3H_4 + H = CH_3CCH_2$	1.66×10^{47}	−10.58	13,690	1 atm, [24]
50	$pC_3H_4 + H = aC_3H_5$	4.91×10^{60}	−14.37	31,644	1 atm, [24]
51	$pC_3H_4 + O = HCCO + CH_3$	7.30×10^{12}		2,250	*i*
52	$pC_3H_4 + O = C_2H_4 + CO$	1.00×10^{13}		2,250	*i*
53	$pC_3H_4 + OH = C_3H_3 + H_2O$	1.00×10^{06}	2.0	100	[32]
54	$pC_3H_4 + CH_3 = C_3H_3 + CH_4$	1.80×10^{12}		7,700	*j*, [39]
55	$pC_3H_4 + C_2H = C_2H_2 + C_3H_3$	1.00×10^{13}			[32]
56	$pC_3H_4 + C_6H_5 = C_3H_3 + C_6H_6$	2.00×10^{12}		15,000	estimated
57	$C_3H_3 + H = aC_3H_4$	2.50×10^{12}			see text
58	$CH_3 + C_2H_2 = aC_3H_4 + H$	5.14×10^{09}	0.86	22,153	1 atm, [24]
59	$aC_3H_4 + H = C_3H_3 + H_2$	1.30×10^{06}	2.0	5,500	$k_{59} = k_{47}$
60	$aC_3H_4 + H = CH_3CCH_2$	9.46×10^{42}	−9.43	11,190	1 atm, [24]
61	$aC_3H_4 + H = aC_3H_5$	1.52×10^{59}	−13.54	26,949	1 atm, [24]
62	$aC_3H_4 + O = C_2H_4 + CO$	2.00×10^{07}	1.8	1,000	[23]
63	$aC_3H_4 + OH = C_3H_3 + H_2O$	5.30×10^{06}	2.0	2,000	[32]
64	$aC_3H_4 + CH_3 = C_3H_3 + CH_4$	1.30×10^{12}		7,700	*j*, [39]
65	$aC_3H_4 + C_2H = C_2H_2 + C_3H_3$	1.00×10^{13}			[32]
66	$aC_3H_4 + C_6H_5 = C_3H_3 + C_6H_6$	2.00×10^{12}		15,000	estimated
	Reactions of propargyl				
67	$C_3H_2 + H = C_3H_3$	1.00×10^{13}			estimated
68	$C_3H_3 + H = C_3H_2 + H_2$	5.00×10^{13}		1,000	[40]
69	$C_3H_3 + O = CH_2O + C_2H$	2.00×10^{13}			[41]
70	$C_3H_3 + OH = C_3H_2 + H_2O$	2.00×10^{13}			[41]
71	$C_3H_3 + O_2 = CH_2CO + HCO$	3.00×10^{10}		2,868	[42]
72	$C_3H_3 + HO_2 = OH + CO + C_2H_3$	8.00×10^{11}			estimated
73	$C_3H_3 + HO_2 = aC_3H_4 + O_2$	3.00×10^{11}			estimated
74	$C_3H_3 + HO_2 = pC_3H_4 + O_2$	2.50×10^{12}			estimated
75	$C_3H_3 + HCO = aC_3H_4 + CO$	2.50×10^{13}			[32]
76	$C_3H_3 + HCO = pC_3H_4 + CO$	2.50×10^{13}			[32]
77	$C_3H_3 + HCCO = C_4H_4 + CO$	2.50×10^{13}			[32]
78	$C_3H_3 + CH = iC_4H_3 + H$	5.00×10^{13}			[32]
79	$C_3H_3 + CH_2 = C_4H_4 + H$	5.00×10^{13}			[32]
80	$C_3H_3 + C_3H_3 = C_6H_6$	2.00×10^{12}			[24, 32]
81	$C_3H_3 + C_3H_3 = C_6H_5 + H$	5.00×10^{12}			estimated
	Reactions of C_3H_2				
82	$C_3H_2 + O = C_2H_2 + CO$	6.80×10^{13}			[43]
83	$C_3H_2 + OH = HCO + C_2H_2$	6.80×10^{13}			[43]
84	$C_3H_2 + O_2 = HCCO + H + CO$	2.00×10^{12}		1,000	[40]
85	$C_3H_2 + CH = C_4H_2 + H$	5.00×10^{13}			[32]
86	$C_3H_2 + CH_2 = nC_4H_3 + H$	5.00×10^{13}			[32]
87	$C_3H_2 + CH_3 = C_4H_4 + H$	5.00×10^{12}			[32]
88	$C_3H_2 + HCCO = nC_4H_3 + CO$	1.00×10^{13}			[32]

(continued on next page)

TABLE 2, Continued

No.	Reaction[b]	$k = AT^n \exp(-E/RT)$[c] A	n	E	References/Comments
	Reactions of n-propyl				
89	$C_3H_6 + H(+M) = nC_3H_7(+M)$	1.33×10^{13}		3,260	k_∞, *d*
		6.26×10^{38}	−6.66	7,000	k_0
	a = 1.00	T^{***} = 1,000	T^* = 1,310	T^{**} = 48,097	*e*
90	$CH_3 + C_2H_4 = nC_3H_7$	3.30×10^{11}		7,700	[44]
91	$nC_3H_7 + H = C_2H_5 + CH_3$	3.70×10^{24}	−2.92	12,505	1 atm, *k*
92	$nC_3H_7 + H = C_3H_6 + H_2$	1.80×10^{12}			[45]
93	$nC_3H_7 + O = C_2H_5 + CH_2O$	9.60×10^{13}			[45]
94	$nC_3H_7 + OH = C_3H_6 + H_2O$	2.40×10^{13}			[45]
95	$nC_3H_7 + O_2 = C_3H_6 + HO_2$	9.00×10^{10}			[45]
96	$nC_3H_7 + HO_2 = C_2H_5 + OH + CH_2O$	2.40×10^{13}			[45]
97	$nC_3H_7 + HCO = C_3H_8 + CO$	6.00×10^{13}			[45]
98	$nC_3H_7 + CH_3 = CH_4 + C_3H_6$	1.10×10^{13}			[45]
	Reactions of i-propyl				
99	$C_3H_6 + H(+M) = iC_3H_7(+M)$	1.33×10^{13}		1,559	k_∞, *d*
		8.70×10^{42}	−7.5	4,722	k_0
	a = 1.00	T^{***} = 1,000	T^* = 645	T^{**} = 6,844	*e*
100	$iC_3H_7 + H = CH_3 + C_2H_5$	1.40×10^{28}	−3.94	15,916	1 atm, *k*
101	$iC_3H_7 + H = C_3H_6 + H_2$	3.20×10^{12}			[45]
102	$iC_3H_7 + O = CH_3CHO + CH_3$	9.60×10^{13}			[45]
103	$iC_3H_7 + OH = C_3H_6 + H_2O$	2.40×10^{13}			[45]
104	$iC_3H_7 + O_2 = C_3H_6 + HO_2$	1.30×10^{11}			[45]
105	$iC_3H_7 + HO_2 = CH_3CHO + CH_3 + OH$	2.40×10^{13}			[45]
106	$iC_3H_7 + HCO = C_3H_8 + CO$	1.20×10^{14}			[45]
107	$iC_3H_7 + CH_3 = CH_4 + C_3H_6$	2.20×10^{14}	−0.68		[45]
	Reactions of propane				
108	$nC_3H_7 + H(+M) = C_3H_8(+M)$	3.60×10^{13}			k_∞, *k*
		3.01×10^{48}	−9.32	5,834	k_0
	a = 0.498	T^{***} = 1,314	T^* = 1,314	T^{**} = 50,000	*e*
109	$iC_3H_7 + H(+M) = C_3H_8(+M)$	2.40×10^{13}			k_∞, *k*
		1.70×10^{58}	−12.08	11,264	k_0
	a = 0.649	T^{***} = 1,213	T^* = 1,213	T^{**} = 13,370	*e*
110	$CH_3 + C_2H_5(+M) = C_3H_8(+M)$	4.90×10^{14}	−0.5		k_∞, *l*
		6.80×10^{61}	−13.42	6,000	k_0
	a = 1.00	T^{***} = 1,000	T^* = 1,434	T^{**} = 5,329	*e*
111	$C_3H_8 + H = H_2 + nC_3H_7$	1.30×10^{06}	2.54	6,756	[45]
112	$C_3H_8 + H = H_2 + iC_3H_7$	1.30×10^{06}	2.4	4,471	[45]
113	$C_3H_8 + O = nC_3H_7 + OH$	1.90×10^{05}	2.68	3,716	[45]
114	$C_3H_8 + O = iC_3H_7 + OH$	4.76×10^{04}	2.71	2,106	[45]
115	$C_3H_8 + OH = nC_3H_7 + H_2O$	1.40×10^{03}	2.66	527	[45]
116	$C_3H_8 + OH = iC_3H_7 + H_2O$	2.70×10^{04}	2.39	393	[45]
117	$C_3H_8 + O_2 = nC_3H_7 + HO_2$	4.00×10^{13}		50,930	[45]
118	$C_3H_8 + O_2 = iC_3H_7 + HO_2$	4.00×10^{13}		47,590	[45]
119	$C_3H_8 + HO_2 = nC_3H_7 + H_2O_2$	4.76×10^{04}	2.55	16,490	[45]
120	$C_3H_8 + HO_2 = iC_3H_7 + H_2O_2$	9.64×10^{03}	2.6	13,910	[45]
121	$C_3H_8 + CH_3 = CH_4 + nC_3H_7$	9.03×10^{-01}	3.65	7,153	[45]
122	$C_3H_8 + CH_3 = CH_4 + iC_3H_7$	1.51×10^{00}	3.46	5,480	[45]
	Reactions of 1*-butene*				
123	$C_4H_7 + H(+M) = 1\text{-}C_4H_8(+M)$	3.60×10^{13}			k_∞, $k_{123} = k_{108}$
		3.01×10^{48}	−9.32	5,834	k_0
	a = 0.498	T^{***} = 1,314	T^* = 1,314	T^{**} = 50,000	*e*

(continued on next page)

TABLE 2, Continued

No.	Reaction[b]	$k = AT^n \exp(-E/RT)^c$ A	n	E	References/Comments
	Reactions of 1-*butene continued*				
124	$aC_3H_5 + CH_3(+M) = 1\text{-}C_4H_8(+M)$	1.00×10^{14}	−0.32	−262	k_∞, *m*
		3.51×10^{60}	−12.97	6,000	k_0
	$a = 0.896$	$T^{***} = 60{,}000$	$T^* = 1{,}606$	$T^{**} = 6{,}118$	*e*
125	$C_2H_3 + C_2H_5(+M) = 1\text{-}C_4H_8(+M)$	1.50×10^{13}			k_∞, *n*
		1.55×10^{56}	−11.79	8,985	k_0
	$a = 0.198$	$T^{***} = 2{,}278$	$T^* = 60{,}000$	$T^{**} = 5{,}723$	*e*
126	$1\text{-}C_4H_8 + H = C_2H_4 + C_2H_5$	1.60×10^{22}	−2.39	11,180	1 atm, $k_{126} = k_3$
127	$1\text{-}C_4H_8 + H = C_3H_6 + CH_3$	3.20×10^{22}	−2.39	11,180	1 atm, $k_{127} = 2 \times k_3$
128	$1\text{-}C_4H_8 + H = C_4H_7 + H_2$	6.50×10^{05}	2.54	6,756	$k_{128} = k_{111}/2$
129	$1\text{-}C_4H_8 + O = nC_3H_7 + HCO$	3.30×10^{08}	1.45	−402	*o*
130	$1\text{-}C_4H_8 + O = C_4H_7 + OH$	1.50×10^{13}		5,760	[46], *p*
		2.60×10^{13}		4,470	*p*
131	$1\text{-}C_4H_8 + OH = C_4H_7 + H_2O$	7.00×10^{02}	2.66	527	$k_{131} = k_{115}/2$
132	$1\text{-}C_4H_8 + O_2 = C_4H_7 + HO_2$	2.00×10^{13}		50,930	$k_{132} = k_{117}/2$
133	$1\text{-}C_4H_8 + HO_2 = C_4H_7 + H_2O_2$	1.50×10^{11}		14,900	estimated
134	$1\text{-}C_4H_8 + CH_3 = C_4H_7 + CH_4$	4.50×10^{-01}	3.65	7,153	$k_{134} = k_{121}/2$
	Reactions of C_4H_7 ($CH_2CHCH_2CH_2$)				
135	$C_4H_7 = 1,3\text{-}C_4H_6 + H$	2.28×10^{52}	−12.01	51,230	1 atm, [32]
136	$C_2H_3 + C_2H_4 = C_4H_7$	7.93×10^{38}	−8.47	14,220	1 atm, [32]
137	$C_4H_7 + H = CH_3 + aC_3H_5$	2.00×10^{21}	−2.0	11,000	estimated
138	$C_4H_7 + H = 1,3\text{-}C_4H_6 + H_2$	1.80×10^{12}			estimated
139	$C_4H_7 + O_2 = 1,3\text{-}C_4H_6 + HO_2$	1.00×10^{11}			estimated
140	$C_4H_7 + HO_2 = CH_2O + OH + aC_3H_5$	2.40×10^{13}			$k_{140} = k_{96}$
141	$C_4H_7 + HCO = 1\text{-}C_4H_8 + CO$	6.00×10^{13}			$k_{141} = k_{97}$
142	$C_4H_7 + CH_3 = 1,3\text{-}C_4H_6 + CH_4$	1.10×10^{13}			$k_{142} = k_{98}$
	Reactions of 1,3-butadiene				
143	$C_2H_3 + C_2H_3 = 1,3\text{-}C_4H_6$	1.50×10^{42}	−8.84	12,483	1 atm, [32]
144	$1,3\text{-}C_4H_6 + H = nC_4H_5 + H_2$	1.33×10^{06}	2.53	12,240	[32]
145	$1,3\text{-}C_4H_6 + H = iC_4H_5 + H_2$	6.65×10^{05}	2.53	9,240	[32]
146	$1,3\text{-}C_4H_6 + H = pC_3H_4 + CH_3$	7.00×10^{12}		2,000	[23]
147	$1,3\text{-}C_4H_6 + O = HCO + aC_3H_5$	6.00×10^{08}	1.45	−860	[47]
148	$1,3\text{-}C_4H_6 + OH = nC_4H_5 + H_2O$	6.20×10^{06}	2.0	3,430	[32]
149	$1,3\text{-}C_4H_6 + OH = iC_4H_5 + H_2O$	3.10×10^{06}	2.0	430	[32]
	Reactions of 1,2-butadiene				
150	$C_3H_3 + CH_3(+M) = 1,2\text{-}C_4H_6(+M)$	1.50×10^{12}			k_∞, *q*
		2.60×10^{57}	−11.94	9,770	k_0
	$a = 0.175$	$T^{***} = 1{,}341$	$T^* = 60{,}000$	$T^{**} = 9{,}770$	*e*
151	$1,2\text{-}C_4H_6 + H = 1,3\text{-}C_4H_6 + H$	2.00×10^{13}		4,000	[32]
152	$1,2\text{-}C_4H_6 + H = iC_4H_5 + H_2$	1.70×10^{05}	2.5	2,490	[32]
153	$1,2\text{-}C_4H_6 + H = aC_3H_4 + CH_3$	2.00×10^{13}		2,000	[32]
154	$1,2\text{-}C_4H_6 + H = pC_3H_4 + CH_3$	2.00×10^{13}		2,000	[23]
155	$1,2\text{-}C_4H_6 + O = CH_2CO + C_2H_4$	1.20×10^{08}	1.65	327	$k_{155} = k_6$
156	$1,2\text{-}C_4H_6 + O = iC_4H_5 + OH$	1.80×10^{11}	0.7	5,880	$k_{156} = k_8$
157	$1,2\text{-}C_4H_6 + OH = iC_4H_5 + H_2O$	3.10×10^{06}	2.0	−298	$k_{157} = k_{10}$
158	$1,2\text{-}C_4H_6 = 1,3\text{-}C_4H_6$	1.00×10^{13}		65,000	1 atm, [32]
	Reactions of nC_4H_5 and iC_4H_5				
159	$nC_4H_5 = iC_4H_5$	1.50×10^{67}	−16.89	59,100	1 atm, [48]
160	$nC_4H_5 + H = iC_4H_5 + H$	3.10×10^{26}	−3.35	17,423	1 atm, [32]
161	$1,3\text{-}C_4H_6 = nC_4H_5 + H$	5.30×10^{44}	−8.62	123,608	1 atm, [32]
162	$nC_4H_5 + H = C_4H_4 + H_2$	1.50×10^{13}			[32]

(continued on next page)

TABLE 2, Continued

No.	Reaction[b]	$k = AT^n \exp(-E/RT)$[c] A	n	E	References/Comments
	Reactions of nC_4H_5 and iC_4H_5 *continued*				
163	$nC_4H_5 + OH = C_4H_4 + H_2O$	2.00×10^{12}			[32]
164	$nC_4H_5 + O_2 \rightarrow C_2H_4 + CO + HCO$	4.16×10^{10}		2,500	[49]
165	$nC_4H_5 + HCO = 1,3\text{-}C_4H_6 + CO$	9.00×10^{13}			[32]
166	$nC_4H_5 + C_2H_2 = C_6H_6 + H$	1.60×10^{16}	−1.33	5,400	1 atm, [48]
167	$iC_4H_5 + H = C_3H_3 + CH_3$	2.00×10^{13}		2,000	[32]
168	$1,3\text{-}C_4H_6 = iC_4H_5 + H$	5.70×10^{36}	−6.27	112,353	1 atm, [32]
169	$iC_4H_5 + H = C_4H_4 + H_2$	3.00×10^{13}			[32]
170	$iC_4H_5 + OH = C_4H_4 + H_2O$	4.00×10^{12}			[32]
171	$iC_4H_5 + O_2 = CH_2CO + C_2H_3O$	7.86×10^{16}	−1.8		[32]
172	$iC_4H_5 + HCO = 1,3\text{-}C_4H_6 + CO$	9.00×10^{13}			[32]
	Reactions of vinylacetylene				
173	$C_4H_4 + H = nC_4H_5$	1.30×10^{51}	−11.92	16,500	1 atm, [48]
174	$C_4H_4 + H = nC_4H_3 + H_2$	6.65×10^{05}	2.53	12,240	[32]
175	$C_4H_4 + H = iC_4H_5$	4.90×10^{51}	−11.92	17,700	1 atm, [48]
176	$C_4H_4 + H = iC_4H_3 + H_2$	3.33×10^{05}	2.53	9,240	[32]
177	$C_4H_4 + OH = nC_4H_3 + H_2O$	3.10×10^{07}	2.0	3,430	[32]
178	$C_4H_4 + OH = iC_4H_3 + H_2O$	1.55×10^{07}	2.0	430	[32]
179	$C_4H_4 + C_2H = lC_6H_4 + H$	1.20×10^{13}			[32]
	Reactions of nC_4H_3 and iC_4H_3				
180	$nC_4H_3 = iC_4H_3$	4.10×10^{43}	−9.49	53,000	1 atm, [48]
181	$nC_4H_3 + H = iC_4H_3 + H$	2.50×10^{20}	−1.67	10,800	1 atm, [32]
182	$nC_4H_3 + H = C_2H_2 + C_2H_2$	6.30×10^{25}	−3.34	10,014	1 atm, [32]
183	$nC_4H_3 + H = C_4H_4$	2.00×10^{47}	−10.26	13,070	1 atm, [32]
184	$nC_4H_3 + H = C_4H_2 + H_2$	3.00×10^{13}			1 atm, [32]
185	$nC_4H_3 + OH = C_4H_2 + H_2O$	2.00×10^{12}			[32]
186	$nC_4H_3 + C_2H_2 = lC_6H_4 + H$	2.50×10^{14}	−0.56	10,600	1 atm, [48]
187	$nC_4H_3 + C_2H_2 = C_6H_5$	9.60×10^{70}	−17.77	31,300	1 atm, [48]
188	$nC_4H_3 + C_2H_2 = cC_6H_4 + H$	6.90×10^{46}	−10.01	30,100	1 atm, [48]
189	$iC_4H_3 + H = C_2H_2 + C_2H_2$	2.80×10^{23}	−2.55	10,780	1 atm, [32]
190	$iC_4H_3 + H = C_4H_4$	3.40×10^{43}	−9.01	12,120	1 atm, [32]
191	$iC_4H_3 + H = C_4H_2 + H_2$	6.00×10^{13}			1 atm, [32]
192	$iC_4H_3 + OH = C_4H_2 + H_2O$	4.00×10^{12}			[32]
193	$iC_4H_3 + O_2 = HCCO + CH_2CO$	7.86×10^{16}	−1.8		[50]
	Reactions of diacetylene				
194	$C_4H_2 + H = nC_4H_3$	1.10×10^{42}	−8.72	15,300	1 atm, [48]
195	$C_4H_2 + H = iC_4H_3$	1.10×10^{30}	−4.92	10,800	1 atm, [48]
196	$C_4H_2 + O = C_3H_2 + CO$	2.70×10^{13}		1,720	[51]
197	$C_4H_2 + OH = H_2C_4O + H$	6.60×10^{12}		−410	[52]
198	$H_2C_4O + H = C_2H_2 + HCCO$	5.00×10^{13}		3,000	[6]
199	$H_2C_4O + OH = CH_2CO + HCCO$	1.00×10^{07}	2.0	2,000	[6]
200	$C_4H_2 + C_2H = C_6H_2 + H$	9.60×10^{13}			[32]
201	$C_4H_2 + C_2H = C_6H_3$	4.50×10^{37}	−7.68	7,100	1 atm, [32]
	Reactions of triacetylene and C_6H_3				
202	$C_6H_2 + H = C_6H_3$	1.10×10^{30}	−4.92	10,800	1 atm, [32]
203	$C_6H_3 + H = C_4H_2 + C_2H_2$	2.80×10^{23}	−2.55	10,780	1 atm, [32]
204	$C_6H_3 + H = lC_6H_4$	3.40×10^{43}	−9.01	12,120	1 atm, [32]
205	$C_6H_3 + H = C_6H_2 + H_2$	3.00×10^{13}			[32]
206	$C_6H_3 + OH = C_6H_2 + H_2O$	4.00×10^{12}			[32]
207	$C_6H_3 + O_2 \rightarrow CO + C_3H_2 + HCCO$	5.00×10^{11}			[32]

(continued on next page)

TABLE 2, Continued

No.	Reaction[b]	$k = AT^n \exp(-E/RT)^c$ A	n	E	References/Comments
	Reactions of $l$$C_6H_4$ (CHCCHCHCCH)				
208	$lC_6H_4 + H = C_6H_5$	1.70×10^{78}	−19.72	31,400	1 atm, [32]
209	$lC_6H_4 + H = cC_6H_4 + H$	1.40×10^{54}	−11.7	34,500	1 atm, [32]
210	$lC_6H_4 + H = C_6H_3 + H_2$	1.33×10^{06}	2.53	9,240	[32]
211	$lC_6H_4 + OH = C_6H_3 + H_2O$	3.10×10^{06}	2.0	430	[32]
	Reactions of benzene and phenyl				
212	$cC_6H_4 + H = C_6H_5$	2.40×10^{60}	−13.66	29,500	1 atm, [32]
213	$C_6H_6 + H = C_6H_5 + H_2$	2.50×10^{14}		16,000	[53]
214	$C_6H_6 + OH = C_6H_5 + H_2O$	1.60×10^{08}	1.42	1,450	[37]
215	$C_6H_5 + H(+M) = C_6H_6(+M)$	1.00×10^{14}			k_∞, [32]
		6.60×10^{75}	−16.3	7,000	k_0
	$a = 1.00$	$T^{***} = 0.10$	$T^* = 585$	$T^{**} = 6{,}113$	e
216	$C_6H_6 + O = C_6H_5O + H$	2.20×10^{13}		4,530	[37]
217	$C_6H_6 + OH = C_6H_5OH + H$	1.30×10^{13}		10,600	[37]
218	$C_6H_5 + O_2 = C_6H_5O + O$	2.60×10^{13}		6,120	[54]
	Reactions of phenoxyl				
219	$C_6H_5O = CO + C_5H_5$	7.41×10^{11}		43,900	[54]
220	$C_6H_5O + H = CO + C_5H_6$	3.00×10^{13}			[32]
221	$C_6H_5O + O = HCO + 2C_2H_2 + CO$	3.00×10^{13}			[32]
222	$C_6H_5O + H(+M) = C_6H_5OH(+M)$	2.50×10^{14}			k_∞, [27]
		1.00×10^{94}	−21.84	13,880	k_0
	$a = 0.043$	$T^{***} = 304$	$T^* = 60{,}000$	$T^{**} = 5{,}896$	e
	Reactions of phenol				
223	$C_6H_5OH + H = C_6H_5O + H_2$	1.15×10^{14}		12,400	[55]
224	$C_6H_5OH + O = C_6H_5O + OH$	2.80×10^{13}		7,352	[56]
225	$C_6H_5OH + OH = C_6H_5O + H_2O$	6.00×10^{12}			[55]
	Reactions of cyclopentadienyl and its derivatives				
226	$C_5H_5 + H(+M) = C_5H_6(+M)$	1.00×10^{14}			k_∞, [27]
		4.40×10^{80}	−18.28	12,994	k_0
	$a = 0.068$	$T^{***} = 401$	$T^* = 4{,}136$	$T^{**} = 5{,}502$	e
227	$C_5H_5 + O = nC_4H_5 + CO$	1.00×10^{14}			[56]
228	$C_5H_5 + OH = C_5H_4OH + H$	5.00×10^{12}			[32]
229	$C_5H_5 + HO_2 = C_5H_5O + OH$	3.00×10^{13}			[56]
230	$C_5H_6 + H = C_5H_5 + H_2$	2.20×10^{08}	1.77	3,000	[56]
231	$C_5H_6 + O = C_5H_5 + OH$	1.80×10^{13}		3,080	[56]
232	$C_5H_6 + OH = C_5H_5 + H_2O$	3.43×10^{09}	1.18	−447	[56]
233	$C_5H_5O = nC_4H_5 + CO$	2.50×10^{11}		43,900	[56]
234	$C_5H_5O + H = CH_2O + 2C_2H_2$	3.00×10^{13}			[32]
235	$C_5H_5O + O = CO_2 + nC_4H_5$	3.00×10^{13}			[32]
236	$C_5H_4OH = C_5H_4O + H$	2.10×10^{13}		48,000	[56]
237	$C_5H_4OH + H = CH_2O + 2C_2H_2$	3.00×10^{13}			[32]
238	$C_5H_4OH + O = CO_2 + nC_4H_5$	3.00×10^{13}			[32]
239	$C_5H_4O = CO + C_2H_2 + C_2H_2$	1.00×10^{15}		78,000	[56]
240	$C_5H_4O + O = CO_2 + 2C_2H_2$	3.00×10^{13}			[32]
	Reactions of acetaldehyde				
241	$CH_3 + HCO = CH_3CHO$	1.80×10^{13}			k_∞, [35]
242	$CH_3CHO + H = CH_3CO + H_2$	4.10×10^{09}	1.16	2,400	[37]
243	$CH_3CHO + O = CH_3CO + OH$	5.80×10^{12}		1,800	[37]
244	$CH_3CHO + OH = CH_3CO + H_2O$	2.35×10^{10}	0.73	−1,110	[37]
245	$CH_3CHO + O_2 = CH_3CO + HO_2$	3.00×10^{13}		39,100	[37]
246	$CH_3CHO + CH_3 = CH_3CO + CH_4$	2.00×10^{-06}	5.6	2,460	[37]

(continued on next page)

TABLE 2, Continued

No.	Reaction[b]	$k = AT^n \exp(-E/RT)^c$ A	n	E	References/Comments
	Reactions of CH_3CO				
247	$CH_3 + CO(+M) = CH_3CO(+M)$	4.85×10^{07}	1.65	6,150	k_∞, *r*
		7.80×10^{30}	−5.39	8,600	k_0
	$a = 0.258$	$T^{***} = 598$	$T^* = 21{,}002$	$T^{**} = 1{,}773$	*e*
248	$CH_3CO + H = CH_3 + HCO$	9.60×10^{13}			[35]
249	$CH_3CO + O = CH_2CO + OH$	3.90×10^{13}			[37]
250	$CH_3CO + O = CH_3 + CO_2$	1.50×10^{14}			[37]
251	$CH_3CO + OH = CH_2CO + H_2O$	1.20×10^{13}			[35]
252	$CH_3CO + OH = CH_3 + CO + OH$	3.00×10^{13}			[35]
253	$CH_3CO + HO_2 = CH_3 + CO_2 + OH$	3.00×10^{13}			[35]
254	$CH_3CO + H_2O_2 = CH_3CHO + HO_2$	1.80×10^{11}		8,226	[35]
	Reactions of C_2H_3O (CH_2CHO)				
255	$C_2H_3O = CH_3 + CO$	7.80×10^{41}	−9.15	46,900	1 atm, *r*
256	$CH_2CO + H(+M) = C_2H_3O(+M)$	3.30×10^{14}	−0.06	8,500	k_∞, *r*
		3.80×10^{41}	−7.64	11,900	k_0
	$a = 0.337$	$T^{***} = 1707$	$T^* = 3{,}200$	$T^{**} = 4{,}131$	*e*
257	$C_2H_3O + H = CH_2CO + H_2$	3.00×10^{13}			[32]
258	$C_2H_3O + O = CH_2O + HCO$	1.00×10^{14}			[57]
259	$C_2H_3O + O = CH_2CO + OH$	1.00×10^{13}			[32]
260	$C_2H_3O + OH = CH_2CO + H_2O$	5.00×10^{12}			[32]
261	$C_2H_3O + O_2 = CH_2CO + HO_2$	1.40×10^{11}			[37]
262	$C_2H_3O + O_2 = CH_2O + CO + OH$	1.80×10^{10}			[37]
263	$C_2H_3O + CH_3 = C_2H_5 + HCO$	4.90×10^{14}	−0.5		[57]
	Additional C_1H_x *and* C_2H_x *reactions not included in the GRI-Mech*				
264	$CH_3 + HCCO = C_2H_4 + CO$	5.00×10^{13}			[32]
265	$CH_3 + C_2H = C_3H_3 + H$	2.41×10^{13}			[35]
266	$CH_4 + C_2H = C_2H_2 + CH_3$	1.81×10^{12}		500	[35]
267	$C_2H_2 + CH = C_3H_2 + H$	3.00×10^{13}			[43]
268	$C_2H_2 + CH_2 = C_3H_3 + H$	1.20×10^{13}		6,620	[58]
269	$C_2H_2 + CH_2^* = C_3H_3 + H$	2.00×10^{13}			[32]
270	$C_2H_2 + C_2H = C_4H_2 + H$	9.60×10^{13}			[48]
271	$C_2H_2 + C_2H = nC_4H_3$	4.50×10^{37}	−7.68	7,100	1 atm, [48]
272	$C_2H_2 + C_2H = iC_4H_3$	2.60×10^{44}	−9.47	14,650	1 atm, [48]
273	$C_2H_2 + C_2H_3 = C_4H_4 + H$	2.00×10^{18}	−1.68	10,600	1 atm, [48]
274	$C_2H_2 + C_2H_3 = nC_4H_5$	9.30×10^{38}	−8.76	12,000	1 atm, [48]
275	$C_2H_2 + C_2H_3 = iC_4H_5$	1.60×10^{46}	−10.98	18,600	1 atm, [48]
276	$C_2H_4 + C_2H = C_4H_4 + H$	1.20×10^{13}			[35]
277	$C_2H_4 + C_2H_3 = 1,3\text{-}C_4H_6 + H$	2.80×10^{21}	−2.44	14,720	1 atm, [32]
278	$C_2H_2 + HCCO = C_3H_3 + CO$	1.00×10^{11}		3,000	[41]
279	$C_2H_4 + O_2 = C_2H_3 + HO_2$	4.22×10^{13}		60,800	[32]
280	$C_2H_3 + H_2O_2 = C_2H_4 + HO_2$	1.21×10^{10}		−596	[35]
281	$C_2H_3 + HCO = C_2H_4 + CO$	9.00×10^{13}			[35]
282	$C_2H_3 + CH_3 = C_2H_2 + CH_4$	3.92×10^{11}			[35]
283	$C_2H_3 + C_2H_3 = iC_4H_5 + H$	1.20×10^{22}	−2.44	13,654	1 atm, [32]
284	$C_2H_3 + C_2H_3 = nC_4H_5 + H$	2.40×10^{20}	−2.04	15,361	1 atm, [32]
285	$C_2H_3 + C_2H_5 = aC_3H_5 + CH_3$	3.90×10^{32}	−5.22	19,747	*n*
286	$CH_2CO + H = CH_3 + CO$	1.50×10^{09}	1.43	2,690	1 atm, *r*
287	$CH_2CO + OH = CH_2O + HCO$	1.00×10^{13}			[37]

[a] The C_1-C_2 chemistry is based on GRI-Mech 1.2 [29] with minor changes as documented in Refs. 30–32, and is not shown in the Table.

[b] Reactions with the "=" sign are reversible, and those with "→" are irreversible.

(continued on next page)

TABLE 2, Continued

[c] Units are in cm, s, mol, and cal.
[d] Fitted to the tabulated values of Tsang [33], assuming $\langle E_{down} \rangle = 600$ cm^{-1}.
[e] Troe's fall-off broadening factor [34], $F_c(T) = (1 - a) \exp(-T/T^{***}) + a \exp(-T/T^{*}) + \exp(-T^{**}/T)$.
[f] Fitted to the tabulated values of Tsang and Hampson [35], assuming $\langle E_{down} \rangle = 600$ cm^{-1}.
[g] Fitted to the tabulated values of Tsang [33], assuming $\langle E_{down} \rangle = 600$ cm^{-1}. The A factor was multiplied by a factor of 2 to better account for the C_2H_4 and CH_4 profiles of propene pyrolysis and oxidation in the flow reactor.
[h] Estimated. $k_{47} = k(C_2H_6 + H = C_2H_5 + H_2)$.
[i] k_{tot} is taken from Ref. 38. The products and branching ratios of reactions 51 and 52 are assumed on the basis of thermochemical considerations [23].
[j] The A factor was reduced from that originally proposed in Ref. 39, 2×10^{12} cm mol^{-1} s^{-1}.
[k] Fitted to the tabulated values of Tsang [45], assuming $\langle E_{down} \rangle = 600$ cm^{-1}.
[l] Fitted to the tabulated values of Refs. 35 and 45, assuming $\langle E_{down} \rangle = 500$ cm^{-1}.
[m] Fitted to the tabulated values of Tsang [33], assuming $\langle E_{down} \rangle = 300$ cm^{-1}.
[n] Fitted to the tabulated values of Tsang and Hampson [35], assuming $\langle E_{down} \rangle = 450$ cm^{-1}.
[o] Fitted to the addition rate coefficient of Ref. 46.
[p] Sum of two rate expressions.
[q] The k_∞ is assumed to be equal to 1.50×10^{12} cm^3/mol-s. The k_0 and F_c parameters are obtained by assuming that k/k_∞ of reaction 150 is equal to that of reaction 2.
[r] Based on unpublished RRKM results with molecular parameter from *ab initio* calculations.

These kinetic data adopted in the present analysis were obtained through an *ab initio* quantum mechanical and Rice-Ramsperger-Kassel-Marcus (RRKM) analysis, followed by comparisons to an extended set of rate data.

The reaction kinetics of propene and allyl were mostly based on the review and compilation of Tsang [33]. In the present model, the unimolecular dissociation of propene is still described by the C-H and C-C fission reactions only, for reasons which will be discussed later. The reactions of allyl + $O_2 \rightarrow$ products and their rate coefficients were taken from the study of Bozzelli and Dean [36], allowing for the multichannel kinetics and pressure dependence of the rate coefficients. The reactions of allyl + $HO_2 \rightarrow$ products and their rate coefficients were taken from Baulch et al. [37]. The reaction kinetics of propane and the propyl radicals were taken from a similar review and compilation by Tsang [45]. The rate coefficients of the propyne and allene unimolecular C-H fission reactions

$$p\text{C}_3\text{H}_4 \rightarrow \text{C}_3\text{H}_3 + \text{H} \qquad (-\text{R45})$$

$$a\text{C}_3\text{H}_4 \rightarrow \text{C}_3\text{H}_3 + \text{H}, \qquad (-\text{R57})$$

were estimated in the present study. These reactions were written in the reverse direction with propyne dissociation being slightly faster than allene dissociation. These rates were consistent with those of Kiefer et al.'s RRKM results [59] at temperatures ~1200 K and pressure ~2 atm. Because of hindered rotation involved in the dissociation process of propyne and allene [59], the pressure fall-off effect in the rate coefficient is not accurately known. Thus we caution that the predictability of the current reaction model may be questionable for propyne and allene pyrolysis at very high temperatures where the pressure fall-off behavior is expected to be significant [24].

The reverse rate of reaction

$$\text{C}_3\text{H}_3 + \text{HO}_2 \rightarrow p\text{C}_3\text{H}_4 + \text{O}_2 \qquad (\text{R74})$$

was estimated and assumed to be similar to that given in Ref. 37 for the reverse of the analogous reaction

$$a\text{C}_3\text{H}_5 + \text{HO}_2 \rightarrow \text{C}_3\text{H}_6 + \text{O}_2. \qquad (\text{R24})$$

The rate coefficient of the second allyl + HO_2 reaction was also taken from Ref. 37. In the current model, we assumed that this second reaction leads to the products given by

$$a\text{C}_3\text{H}_5 + \text{HO}_2 \rightarrow \text{C}_2\text{H}_3 + \text{CH}_2\text{O} + \text{OH}. \qquad (\text{R25})$$

It is likely that the above reaction represents a global reaction step, and the elementary products may include acrolein or there may be an

additional reaction channel that could lead to acrolein formation. We did not include acrolein in the current kinetic model because (a) this species was not found to be a dominant intermediate in our flow reactor experiments, and (b) its reaction kinetics are still largely uncertain. It is noted that acrolein may have to be considered for propene oxidation under ultra fuel-lean stoichiometry [15].

Two C_3H_5 isomers were considered in the kinetic model, including allyl and the propenyl radical CH_3CCH_2. We note that as intermediate species, the CH_3CCH_2 radical and a third isomer CH_3CHCH play an insignificant role in the propene pyrolysis and oxidation under the conditions of experiments considered in the present study. Recognizing that the CH_3CHCH radical is less stable than the CH_3CCH_2 and it participates little in the overall pyrolysis and oxidation processes of C_3H_6, this CH_3CHCH radical isomer is excluded from the current kinetic model.

The thermodynamic data were mostly taken from GRI-Mech 1.2 [29] and from the compilation of Burcat and McBride [60]. The enthalpy of formation of the allyl radical ($\Delta_f H_{298} = 40.9$ kcal/mol) was taken from a recent recommendation by Tsang [61]. The thermochemistry of the CH_3CCH_2 radical was based on our recent theoretical result [24]. The laminar flame speeds were calculated using the Sandia Chemkin-II [62] and PREMIX [63] codes. The ignition delay and flow reactor simulations were conducted using the Senkin code [64]. The computational ignition delay was determined as the maximum in the pressure gradient computed under the constant-density condition.

RESULTS AND DISCUSSION

Propene Pyrolysis

Figure 1 presents the species profiles from the propene pyrolysis experiment conducted in the PTFR. It was found that the temperature did not change by more than 10 K throughout the reactor. Gas chromatography (GC) analysis detected CH_4, C_2H_2, C_2H_4, C_2H_6, pC_3H_4, aC_3H_4, C_3H_6, C_3H_8, 1,3-butadiene (1,3-C_4H_6), vinylacetylene (C_4H_4), butenes, cyclopentadiene, and

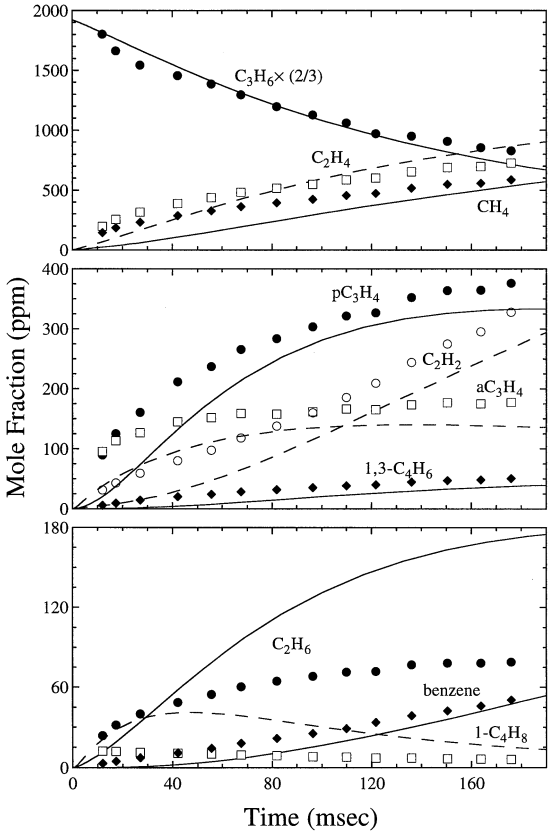

Fig. 1. Experimental (symbols) and computed (lines) mole fraction profiles of major species in the pyrolysis of 0.288% propene in nitrogen in the PTFR at 1 atm, 1210 K.

benzene. It was difficult to obtain a clean separation of vinylacetylene from 1,3-butadiene on the GC, although it is quite clear that the vinylacetylene concentration is significantly smaller than the 1,3-butadiene concentration.

Background levels of oxygen were detected, but never exceeded 150 ppm. It is estimated that these background levels of oxygen never exceeded 60 ppm in the reaction zone of the reactor, and that the remaining oxygen contamination occurred in the carrier lines to the sample valves, where the mixture was already quenched. It was found in our previous study [24] (and confirmed in the present study) that this level of oxygen contamination slightly accelerates the initial reactivity, and is quickly damped out, minimally affecting the remaining reaction process. Despite its negligible effect, oxygen contamination was included in all model calculations. It is seen in Fig. 1 that ethylene and

methane are the two major products of propene pyrolysis at these conditions, followed by propyne, acetylene, and allene. Minor products (<100 ppm) are found to be 1,3-butadiene, ethane, benzene, and 1-butene.

Figure 1 also presents the computed species profiles. To facilitate meaningful comparison between experimental and modeling results, the experimental data were time-shifted by 6 msec to account for nonidealities in the mixing process which tend to accelerate initial fuel consumption, as discussed extensively in Ref. 65. It is seen that all the major species profiles were reproduced well by the present model. However, the model overpredicts the concentrations of a few minor species, including C_2H_6 and 1-C_4H_8 by as much as a factor of 3.

According to the model, the radical pool is initiated through propene dissociation via

$$C_3H_6 = aC_3H_5 + H, \qquad (-R1)$$

whereas propene is largely consumed by hydrogen attack through reactions

$$C_3H_6 + H = C_2H_4 + CH_3 \qquad (R3)$$

$$C_3H_6 + H = aC_3H_5 + H_2. \qquad (R4)$$

Ethylene is predominately formed by reaction (R3), and the formation of methane is controlled by H-atom abstraction by CH_3:

$$C_3H_6 + CH_3 = aC_3H_5 + CH_4 \qquad (R13)$$

$$pC_3H_4 + CH_3 = C_3H_3 + CH_4 \qquad (R54)$$

$$aC_3H_4 + CH_3 = C_3H_3 + CH_4. \qquad (R64)$$

Allene is initially formed by the rapid dissociation of the allyl radical

$$aC_3H_5 = aC_3H_4 + H, \qquad (-R61)$$

followed by a rapid conversion to propyne via the hydrogen-catalyzed as well as direct isomerization reactions

$$aC_3H_4 + H = pC_3H_4 + H \qquad (-R48)$$

$$aC_3H_4 = pC_3H_4. \qquad (-R43)$$

The formation of acetylene is mainly controlled by the chemically activated reaction

$$pC_3H_4 + H = C_2H_2 + CH_3, \qquad (-R46)$$

and by the dissociation of vinyl. Ethane and benzene are formed from the self-recombination of methyl and propargyl, respectively. 1,3-Butadiene is mostly formed from the reverse of the chemically activated reaction

$$1,3\text{-}C_4H_6 + H = pC_3H_4 + CH_3, \qquad (R146)$$

and 1-butene is controlled by the recombination reaction

$$aC_3H_5 + CH_3 = 1\text{-}C_4H_8. \qquad (R124)$$

The overall pyrolysis process is largely governed by a chain-reaction sequence, involving the reactions described above.

Using the original expression of k_3, as suggested by Tsang [33], the model underpredicted the profiles of ethylene and methane. Reaction (R3) is the only notable source of ethylene and the methyl radical, which through reactions (R13), (R54), and (R64) produces methane. We increased k_3 by a factor of 2, a value close to that suggested by Hidaka et al. [22] yet still within the uncertainty quoted in Ref. 33. This increase is also consistent with the work of Thomas et al. [15] who preferred the rates of Ref. 22 for this reaction. As a result of this change, we noticed improvements in the predictions of ethylene and methane profiles for the pyrolysis as well as the oxidation experiments as will be shown later.

An increase in k_3, however, deteriorates the predictions for ethane via

$$CH_3 + CH_3 \rightarrow C_2H_6$$

and 1-butene via (R124). The concentrations of these two species were overpredicted with the original value of k_3. Thus, it was determined that the methyl radical must be slightly overpredicted by the current model, with or without the changes to k_3. It is likely that the problem was caused by the uncertainties in the initiation reactions, which dictate the concentrations of the initial radical pool and species.

Figure 2 shows the ranked sensitivity coefficients for propene at 50% fuel decay. It is seen that propene decay is predominantly dependent on its dissociation to allyl + H (R1), followed by the dissociation of allyl (R61). Because of the importance of the initial dissociation reaction, and the likely overprediction of the methyl

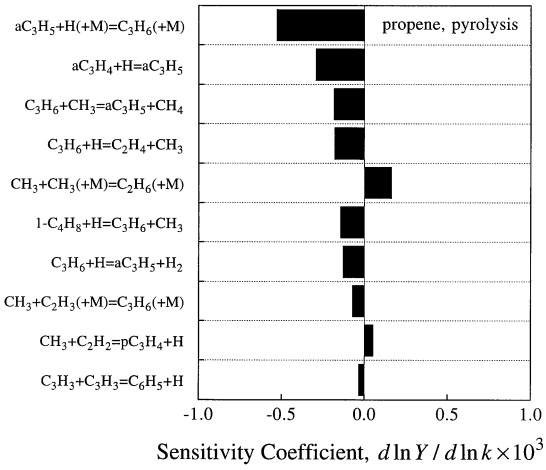

Fig. 2. Logarithmic response sensitivity coefficients of propene concentration at 50% consumption, computed for propene pyrolysis in the flow reactor.

radical concentrations, the unimolecular decomposition of propene deserves further discussion.

The current model includes only the two dissociation pathways as suggested by Tsang [33]

$$C_3H_6 = aC_3H_5 + H \qquad (-R1)$$

$$C_3H_6 = C_2H_3 + CH_3. \qquad (-R2)$$

Following the findings of Hidaka et al. [22], we also included the following reactions.

$$C_3H_6 = C_2H_2 + CH_4$$

$$C_3H_6 = H_2 + pC_3H_4,$$

and adopted the suggested rate coefficients for these four reactions. This led to predictions with mixed results. Specifically, the predictions for C_2H_2, CH_4, C_2H_6, and 1-C_4H_8 were improved; however, the predictions for C_3H_6, C_2H_4, aC_3H_4, and pC_3H_4 worsened.

On the basis of these results, we only included reactions (R1) and (R2) with the rate coefficients of Ref. 33, (a) because these two reactions alone could accurately reproduce the fuel decay and major species profiles in the pyrolysis experiment, and they had only minor influences in the oxidation of propene in the PTFR, and (b) because of inherent kinetic coupling of various rate coefficients for reactions associated with propene pyrolysis. We propose that more

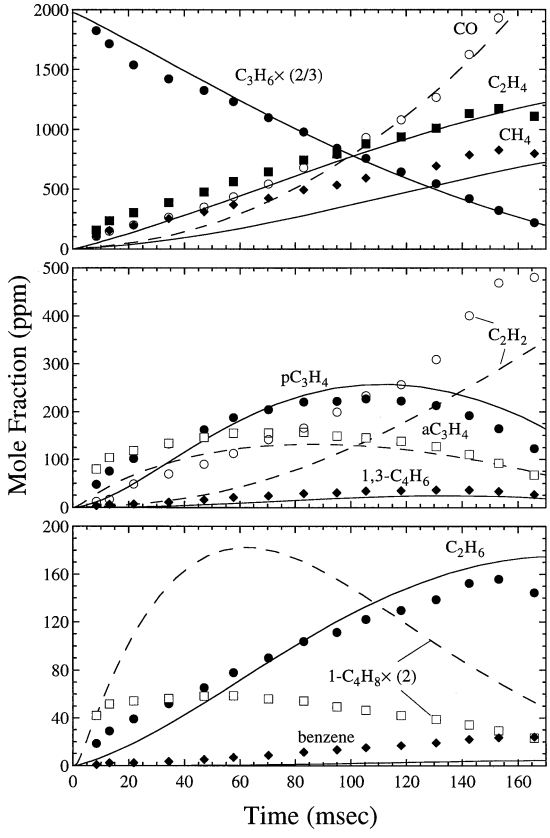

Fig. 3. Experimental (symbols) and computed (lines) mole fraction profiles of major species during propene oxidation (ϕ = 1.0) in the PTFR at 1 atm, 1181 K.

work needs to be conducted in order to fully understand the product distribution of the temperature- and pressure-dependent decomposition reactions. It is, however, worth noting that the rate coefficients determined in Ref. 24 for reactions (R61), (R48), and (R43) accurately describe the species profiles of both allene and propyne at these conditions.

Propene Oxidation in the PTFR

Figures 3, 4, and 5 present the species profiles for propene oxidation in the PTFR for ϕ = 1.0, 0.7, and 1.4, respectively. Hydrocarbon species detected were similar to those found in the pyrolysis experiments with the addition of CO, CO_2, and an unidentified oxygenated species, presumably acrolein, acetaldehyde, or formaldehyde. The maximum concentration of this unidentified species was estimated to be no

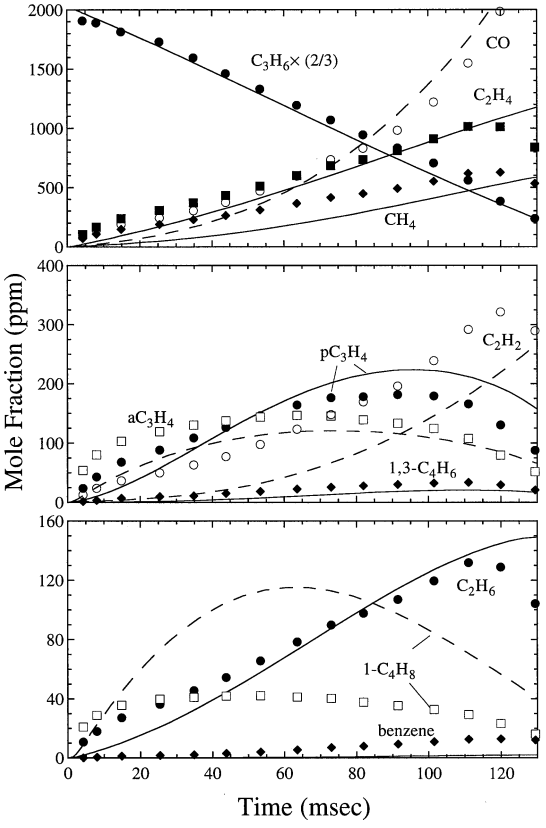

Fig. 4. Experimental (symbols) and computed (lines) mole fraction profiles of major species during propene oxidation (ϕ = 0.7) in the PTFR at 1 atm, 1170 K.

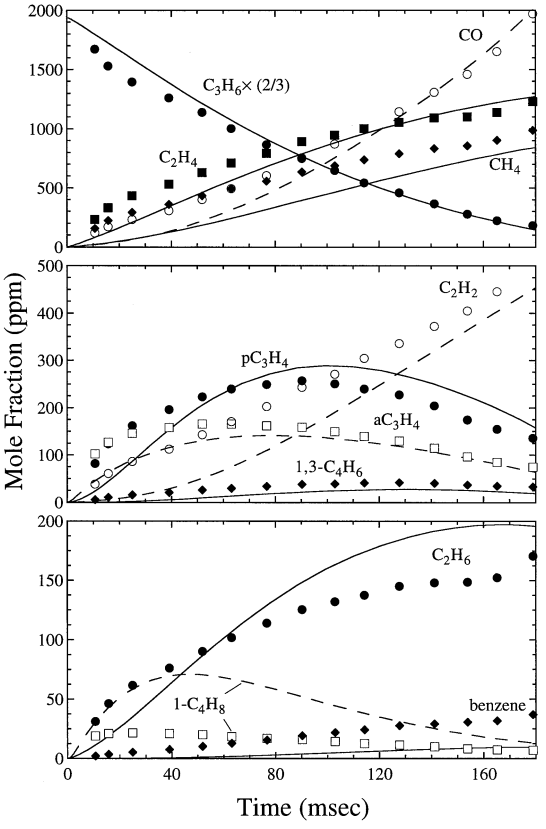

Fig. 5. Experimental (symbols) and computed (lines) mole fraction profiles of major species during propene oxidation (ϕ = 1.4) in the PTFR at 1 atm, 1200 K.

greater than 60 ppm. The modeling results are also presented in these figures. Again the experimental data were time-shifted 3, 0, and 5 msec for ϕ = 1.0, 0.7 and 1.4, respectively. In addition to the species plotted in these figures, the following species were predicted to have significant concentrations but were not measured in the experiment: H_2O, H_2, CH_2O, and CH_2CO with maximum concentration levels at 1500, 800, 200, 150 ppm, respectively, for the stoichiometric mixture.

It is seen in Figs. 3–5 that the model predicts the slope of the fuel decay profiles very well for all mixture stoichiometries, and after appropriate time shifts it also predicts well the shape of the fuel profiles. According to the model, propene is largely consumed by reactions (R3), (R4), and

$$C_3H_6 + OH = aC_3H_5 + H_2O. \qquad (R10)$$

Similar to propene pyrolysis in the PTFR, C_2H_4 is predominately produced from reaction (R3), while CH_4 is formed from (R13), (R54), (R64), and the reaction

$$CH_3 + CH_2O = CH_4 + HCO.$$

Allene is again formed from dissociation of the allyl radical (R61). This is followed by a rapid isomerization to pC_3H_4 via (R43) and (R48). CO is produced from the HCO radical via unimolecular decomposition and its reaction with O_2. Formation of all the other species (C_2H_2, 1,3-C_4H_6, C_6H_6, 1-C_4H_8) is controlled by the same reactions as described in the pyrolysis section.

Figure 6 presents the sensitivity spectrum, computed for propene oxidation in the flow reactor at ϕ = 1.0, which is fairly representative of all equivalence ratios. The sensitivity coefficients of propene concentration were obtained

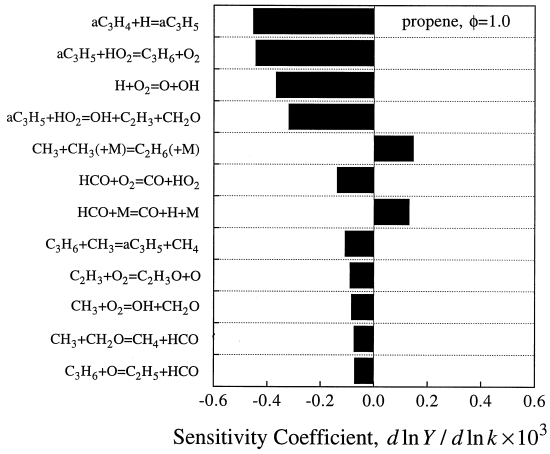

Fig. 6. Logarithmic response sensitivity coefficients of propene concentration at 50% consumption, computed for propene oxidation in the flow reactor at $\phi = 1.0$.

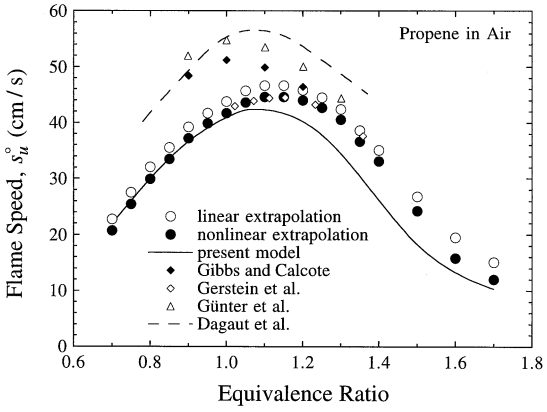

Fig. 7. Comparison of experimental (symbols) laminar flame speeds of propene/air mixtures at 1 atm determined in the present study (linearly and nonlinearly extrapolated) and in previous studies [7–9]. Also shown are the computed flame speeds using the present model (solid line) and that of Ref. 13 (dashed line).

at 50% fuel consumption, and the ranking was similar over the majority of the reaction times. The most influential reaction is the dissociation of the allyl radical (R61), followed by (a) the initiation reaction via the reverse of (R24)

$$aC_3H_5 + HO_2 = C_3H_6 + O_2, \qquad \text{(R24)}$$

(b) the chain-branching reaction of $H + O_2$, and (c) reaction (R25). Similar to propene, the predicted profiles of both allene and propyne were mostly influenced by reaction (R61). The calculated allene and propyne profiles were also very sensitive to the isomerization reactions, (R48) and (R43), and the chemically activated reaction ($-$R46). Consequently, the accurate prediction of propene, allene, and propyne appear to support the values of these rate coefficients as determined in Ref. 24, for the current flow reactor conditions.

It is also seen in Figs. 3–5 that the ethylene profile is predicted quite well by the increased k_3 from the value, which was recommended in Ref. 33. Furthermore, the methyl radical is not overpredicted as can be seen by the accurate prediction of ethane, which is again only formed by the recombination of CH_3. Acetylene and methane are underpredicted during the early stages of reaction; however, following the initiation period their rates of production are well captured. This result provides additional evidence that the inclusion of C_3H_6 dissociation to $C_2H_2 + CH_4$ may provide an additional source of acetylene and methane in the early stages before the radical pool is established. It is seen that 1-butene is overpredicted for all equivalence ratios by a factor of 3–4. Similar to the propene pyrolysis experiment, 1-butene is predominately formed by the recombination of allyl and methyl (R124), again pointing to the uncertainties associated with the unimolecular decomposition of propene previously discussed, and possibly the subsequent reactions of $1\text{-}C_4H_8$.

Laminar Flame Speed of Propene–Air Mixtures

Figure 7 presents the linearly and nonlinearly extrapolated flame speed data for propene/air mixtures. The nonlinear results are ~1–2 cm/s lower than those obtained from the linear extrapolation. The peak in the flame speed data is found to occur near an equivalence ratio of about $\phi = 1.1$. Figure 7 also compares the present laminar flame speeds with the Bunsen flame results of Gibbs and Calcote [7] and Günther and Janisch [9], and the data of Gerstein et al. [8] which were obtained using flame propagation in a tube. It is noted that there is a substantial disagreement in the flame speed data obtained from these previous experiments, and that the previously determined flame speeds can differ quite substantially when com-

pared to the present stretch-compensated flame speed data. Specifically, since the Bunsen flame technique used by Gibbs and Calcote [7] and Günther and Janisch [9] suffer from stretch effects, their data exhibit tendencies relative to the present data which are supported by flame stretch theory [25, 27]. The maximum difference between the present data and those of Refs. 7 and 9 is as large as 10–15 cm/s. Interestingly though, the data of Gerstein et al. [8] agree quite well with the present data despite the expected wall effects, including heat loss and radical scavenging, and the notable influence that stretch coupled with mixture nonequidiffusion has on the measured flame speeds.

The present kinetic model predicts reasonably well the shape of the flame speed curve, but it underpredicts the experimental data at stoichiometric to fuel-rich equivalence ratios. Figure 7 also presents the model predictions of Dagaut et al. [13], which were originally compared to the flame speed data of Refs. 7 and 9. The significant difference between the previous and present data further confirms the need for accurate, stretch-compensated flame speed data for validating kinetic models.

According to the present model, the kinetics governing propene oxidation in laminar premixed flames is very similar to that in the flow reactor, with a few notable differences. Because of the abundance of H-atoms, reaction (R1) proceeds in the recombination direction, and the hydrogen-catalyzed isomerization of allene to propyne (−R48) is more important than its direct isomerization (−R43).

A detailed sensitivity analysis was also performed and the result is presented in Fig. 8. It is seen that the ranked sensitivity spectrum is populated with a few reactions of propene which influence flame speed, namely (R1), (R3), (R4), and (R10). Within the uncertainty limits in the rate coefficients of these reactions and without simultaneously deteriorating flow reactor predictions, it is not possible to further improve flame speed predictions at rich equivalence ratios. We note that to improve the prediction at fuel-rich stoichiometries, it may be necessary to take into account the formation of higher molecular weight species. In addition,

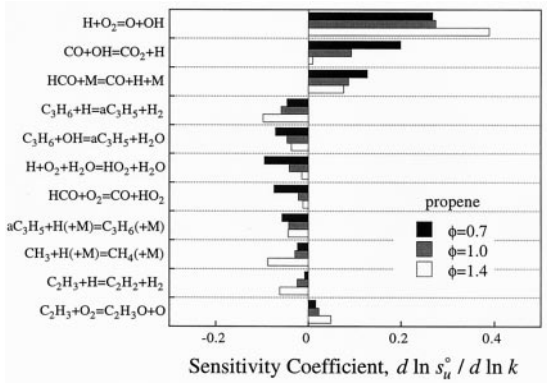

Fig. 8. Logarithmic response sensitivity coefficients of flame speed computed for propene/air at the equivalence ratios of 0.7, 1.0, and 1.4.

the disagreement is also indicative of the lack of understanding concerning the dissociation reactions of propene.

Shock-Tube Ignition of Propene

Comparisons were also made between predicted and experimentally measured [10] ignition delays for propene–oxygen–argon mixtures, using the present kinetic model. The computational results were less than adequate, predicting ignition delays shorter than the experimental data for all conditions. The results were fairly close at lower temperatures (~1250–1450 K) and for stoichiometric to fuel-lean conditions; however, the predicted ignition delay times were lower than the experimental data by a factor of 3 at higher temperatures (1550–2000 K) and fuel-rich conditions. The computed ignition delays were very sensitive to the propene unimolecular decomposition reactions, and, within the uncertainties quoted in Ref. 33, the predictions could not be improved. The propene dissociation channels and rate coefficients as suggested by Hidaka et al. [22] were also tested, but with very little improvement. Again, it is likely that the temperature- and pressure-dependent rate coefficients for propene unimolecular decomposition reactions need to be examined further in order to resolve the discrepancies between experiment and kinetic mechanism.

TABLE 3

Initial Conditions for Propyne Oxidation in the PTFR

	Mole Fraction			
ϕ	pC_3H_4	O_2	N_2	T_o (K)
0.7	0.00312	0.01784	0.97904	1170
1.0	0.00307	0.01229	0.98464	1170
1.4	0.00303	0.00864	0.98833	1174

Propyne Oxidation in the PTFR

The experimental data of propyne oxidation in the PTFR were collected for the equivalence ratios of 0.7, 1.0, and 1.4 [23]. The initial mixture compositions and temperatures are given in Table 3. The fuel decay profiles for the three equivalence ratios and species profiles for the stoichiometric case were previously reported in Ref. 23. Here, we report species profiles collected under all conditions, as seen in Figs. 9–11, as well as the modeling results with the present kinetic model, which includes revisions on the basis of our recent theoretical results [24].

The experimental data shown in Figs. 9–11 were time shifted by 5, 1, and 2 msec for ϕ = 1.0, 0.7, and 1.4, respectively. The model predicts fairly well the fuel decay profile as well as other major species profiles, with the exception of ethane and ethylene. According to the model, propyne initially forms allene through its direct isomerization

$$pC_3H_4 = aC_3H_4, \qquad \text{(R43)}$$

and at later residence times by both reaction (R43) and

$$pC_3H_4 + H = aC_3H_4 + H. \qquad \text{(R48)}$$

Propyne is also largely consumed by H-atom attack via

$$pC_3H_4 + H = C_2H_2 + CH_3, \qquad (-\text{R46})$$

which is the primary source of acetylene and the methyl radical. Allene is consumed mainly through H abstraction by OH, producing C_3H_3. Methane is predominately formed by H abstraction by CH_3 from propyne and allene,

$$pC_3H_4 + CH_3 = C_3H_3 + CH_4 \qquad \text{(R54)}$$

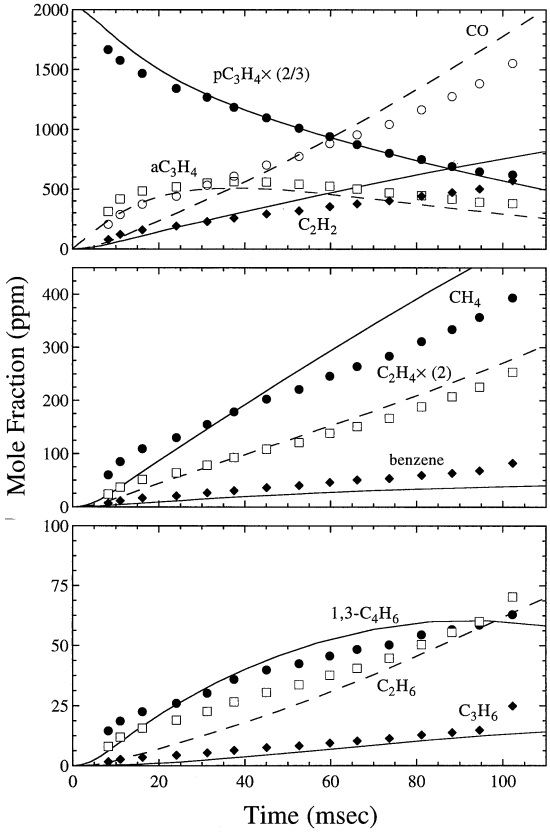

Fig. 9. Experimental (symbols, [23]) and computed (lines) mole fraction profiles of major species during propyne oxidation (ϕ = 1.0) in the PTFR at 1 atm, 1170 K.

$$aC_3H_4 + CH_3 = C_3H_3 + CH_4. \qquad \text{(R64)}$$

Ethylene is produced by the chemically activated reaction of O-atom with propyne and allene

$$pC_3H_4 + O = C_2H_4 + CO \qquad \text{(R52)}$$

$$aC_3H_4 + O = C_2H_4 + CO. \qquad \text{(R62)}$$

The products of these reactions were assigned on the basis of thermochemical consideration [23].

Similar to the propene system, ethane is formed from the recombination of methyl, whereas benzene is produced from propargyl recombination. CO is produced from the HCO radical via unimolecular decomposition and its reaction with molecular oxygen. The formyl radical is produced mainly through

$$C_3H_3 + O_2 = CH_2CO + HCO. \qquad \text{(R71)}$$

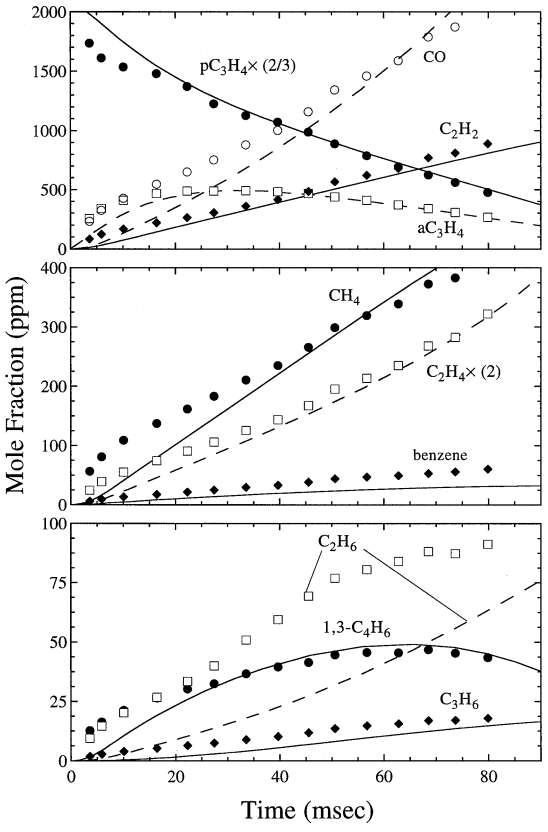

Fig. 10. Experimental (symbols) and computed (lines) mole fraction profiles of major species during propyne oxidation (ϕ = 0.7) in the PTFR at 1 atm, 1170 K.

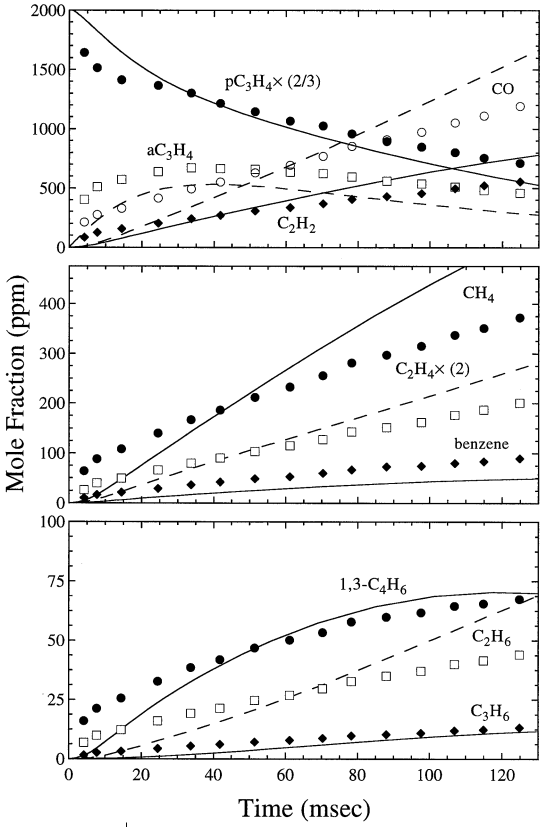

Fig. 11. Experimental (symbols) and computed (lines) mole fraction profiles of major species during propyne oxidation (ϕ = 1.4) in the PTFR at 1 atm, 1174 K.

1,3-Butadiene is largely produced by the reverse of reaction (R146), and is consumed by its reactions with H, O, and OH via

$$1,3\text{-}C_4H_6 + H = C_2H_4 + C_2H_3 \qquad (-R277)$$

$$1,3\text{-}C_4H_6 + O = aC_3H_5 + HCO \qquad (R147)$$

$$1,3\text{-}C_4H_6 + OH = nC_4H_5 + H_2O \qquad (R148)$$

$$1,3\text{-}C_4H_6 + OH = iC_4H_5 + H_2O. \qquad (R149)$$

Figure 12 shows the ranked sensitivity coefficients for propyne oxidation in the flow reactor for ϕ = 1.0, which is representative of all three cases. The sensitivity coefficients were obtained at 50% fuel consumption. For the present calculation reactions describing the recombination of the propargyl radical,

$$C_3H_3 + C_3H_3 = C_6H_6 \qquad (R80)$$

$$C_3H_3 + C_3H_3 = C_6H_5 + H, \qquad (R81)$$

are among the most influential reactions for the fuel profile. Reaction (R81) serves to accelerate

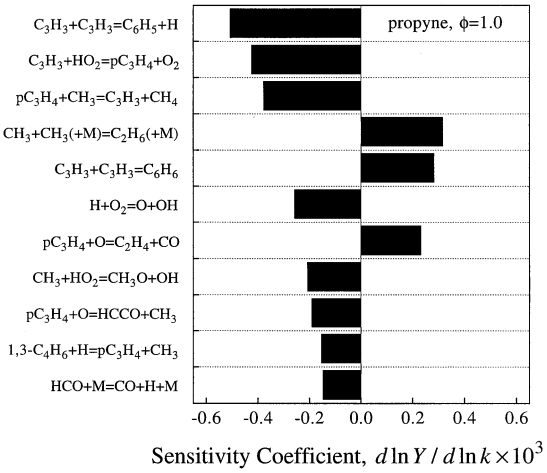

Fig. 12. Logarithmic response sensitivity coefficients of propyne concentration at 50% consumption, computed for propyne oxidation in the flow reactor at ϕ = 1.0.

fuel consumption by adding H atoms into the system where reaction (R80) is inhibiting due to radical-chain termination. The branching ratio of these two reactions was estimated from our previous study [24] and it does fairly well at predicting the fuel decay profile and the reactivity of the system in general. Benzene profiles also seem to be reasonably predicted by these rates; however, it should be noted that products and distributions of the propargyl recombination reaction are far from being resolved [59]. In particular, fulvene may have to be considered as an intermediate to benzene [66]. The obvious consequence is that the branching ratio for global reactions (R80) and (R81) must be temperature- and pressure-dependent.

It is also noticed that the reactions

$$p\mathrm{C_3H_4} + \mathrm{O_2} = \mathrm{C_3H_3} + \mathrm{HO_2} \qquad (-\mathrm{R74})$$

$$p\mathrm{C_3H_4} + \mathrm{CH_3} = \mathrm{C_3H_3} + \mathrm{CH_4}, \qquad (\mathrm{R54})$$

along with the recombination of the methyl radical forming ethane, are also very influential under the present conditions. Reaction (−R74) initiates fuel consumption and its rate was estimated based on the analogous propene reaction. A slight reduction of this rate improves the predictions of the fuel decay profile, especially for rich conditions; however, this rate also represents a compromise between the flow reactor and ignition delay predictions which will be discussed subsequently. Furthermore, the current product assignment and rate coefficients of $p\mathrm{C_3H_4}$ + O and $a\mathrm{C_3H_4}$ + O reactions seem to do reasonably well at predicting the ethylene profiles under flow reactor conditions.

Laminar Flame Speed of Propyne–Air Mixtures

Figure 13 presents the linearly and nonlinearly extrapolated flame speeds for propyne/(18%O_2 in N_2) mixtures [23], as well as the predictions using the current kinetic model. It is seen that the present kinetic model predicts reasonably well the shape and magnitude of the flame speed curve. Using the recently determined rate coefficients as suggested in Ref. 24, the predictions of the flame speed curve show an improvement over those previously reported

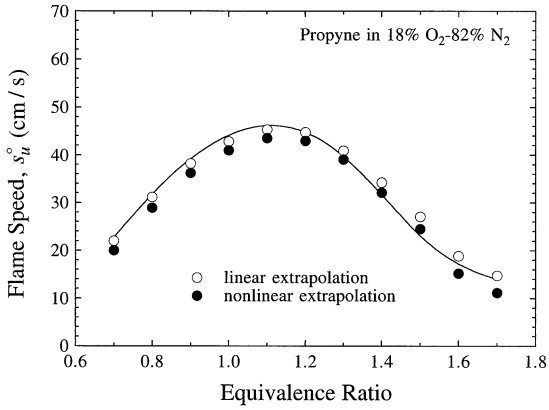

Fig. 13. Comparison of experimental (symbols, [23]) and computed (line) laminar flame speeds of propyne in nitrogen-diluted air (18%O_2–82%N_2) at 1 atm.

[23]. Based on the model, the consumption of propyne in laminar premixed flames is mainly due to reaction (−R46), followed by the hydrogen-catalyzed isomerization to allene (R48). A detailed sensitivity analysis was also performed and the most influential reactions for the propyne flame speeds are found to be the reactions of hydrogen and C_1 hydrocarbon species.

Shock-Tube Ignition of Propyne and Allene

The present kinetic model was tested against the ignition delay data of Curran et al. [67], obtained for the $p\mathrm{C_3H_4}$–$\mathrm{O_2}$–Ar and $a\mathrm{C_3H_4}$–$\mathrm{O_2}$–Ar mixtures behind reflected shock waves. Figure 14 presents the comparison between experimental data and model predictions for mixtures of 1% propyne + X% oxygen at a fixed pressure (3.5 atm), where X = 2, 4, 8 correspond to ϕ = 2.0, 1.0, 0.5, respectively. Figure 15 presents a similar comparison for mixtures of 1% allene + X% oxygen at 2.1 atm. The model, for most conditions, predicts the ignition delay data for both fuels reasonably well. For propyne, the predictions for the X = 2, 4 cases were in good agreement with the experimental ignition delay whereas the predictions for lean conditions (X = 8) were slightly higher throughout the experimental temperature range. Similar but opposite results were noticed for the ignition delay of allene, where fairly good agreement was achieved for the X =

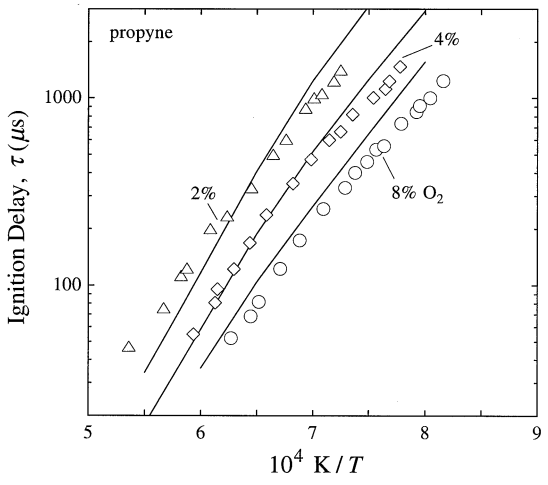

Fig. 14. Experimental (symbols, [67]) and computed (lines) ignition delay times for mixtures of 1% propyne, X% oxygen, and $(99 - X)$% argon at the pressure of 3.5 atm, where $X = 2$, 4, and 8 correspond to the equivalence ratios of 2.0, 1.0, and 0.5, respectively.

4, 8 cases and under rich conditions ($X = 2$) predictions are slightly lower for most of the temperature range.

With the exception of one mixture, the ignition delay times computed at lower temperatures tend to be larger than the experimental data. To examine the possible impurity effect, we performed ignition-delay calculations by adding known amounts of impurities [67] to propyne and allene. The results showed that the ignition delay times were minimally affected (<2%), even at the lowest temperature shown in Figs. 14 and 15. Hence the disagreement between model and experiment at the low-temperature end cannot be accounted for by any impurity effects.

Figures 16 and 17 respectively show the sensitivity spectrum of ignition delay times for 1% propyne and 1% allene in 4% oxygen and 95% argon at 3.5 atm. These conditions are fairly

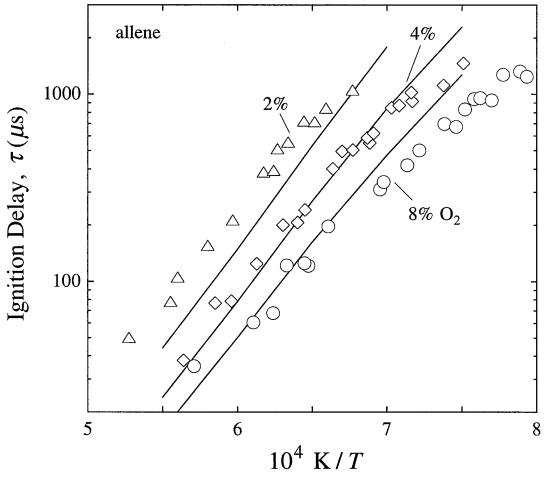

Fig. 15. Experimental (symbols, [67]) and computed (lines) ignition delay times for mixtures of 1% allene, X% oxygen, and $(99 - X)$% argon at the pressure of 2.1 atm, where $X = 2$, 4, and 8 correspond to the equivalence ratios of 2.0, 1.0, and 0.5, respectively.

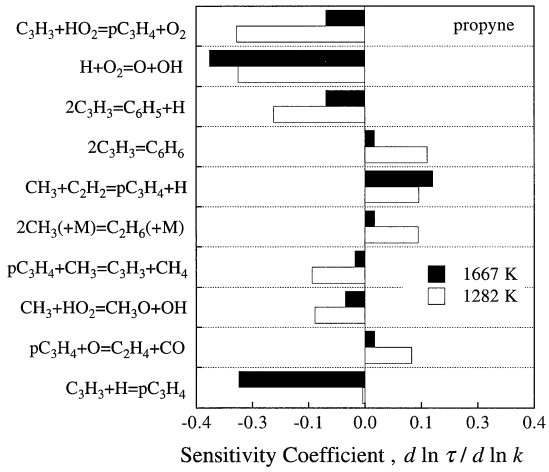

Fig. 16. Logarithmic response sensitivity coefficients of ignition delay of 1% propyne, 4% oxygen, and 95% argon mixture at the pressure of 3.5 atm and temperatures of 1282 and 1667 K.

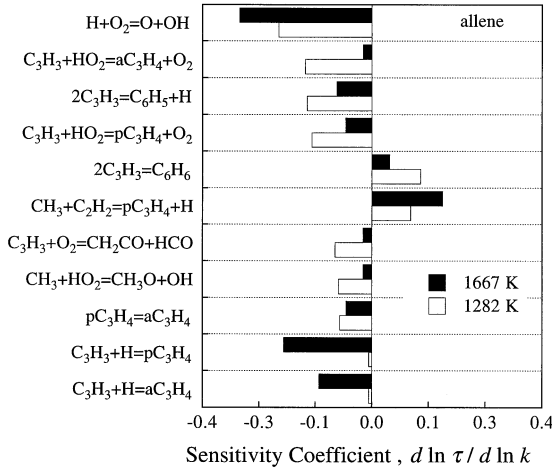

Fig. 17. Logarithmic response sensitivity coefficients of ignition delay of 1% allene, 4% oxygen, and 95% argon mixture at the pressure of 3.5 atm and temperatures of 1282 and 1667 K.

representative of the ranges of equivalence ratios and pressures studied. At lower temperatures the ignition delay of propyne is mostly sensitive to the initiation reaction (−R74), the reaction H + O_2 = O + OH, and the recombination of C_3H_3 (R80, R81). Reaction (−R74) is also extremely influential under lean conditions (X = 8) which are not shown. An increase in k_{74} improves the model predictions for fuel-lean and low-temperature conditions; however, this same increase has an adverse effect under flow reactor conditions where the predicted fuel decay proceeds much too quickly. Therefore, as mentioned earlier, the rate of reaction (−R74) represents a compromise between ignition delay and flow reactor predictions, and the lack of agreement is likely due to the coupling of many influential reactions.

At higher temperatures, the ignition delay of propyne is mostly influenced by the H + O_2 = O + OH reaction, the unimolecular C-H fission of propyne (−R45), and to a lesser extent propyne destruction through H-atom attack (−R46). Ignition delay for allene at high temperatures is also sensitive to this same set of reactions with an added sensitivity to the unimolecular C-H fission of allene (−R57). These same reactions were also the most influential for the ignition delay of allene under rich conditions (X = 2, 2.1 atm). For this case (Fig. 15), the predictions agree at the lowest temperature while becoming progressively worse with an increase in temperature. This may be a result of both C-H fission reactions (−R45, −R57) not including fall-off in their estimations. Including fall-off for these reactions is, however, not simple [65] and is left for future work. It should be noticed that ignition delay for both propyne and allene is sensitive to many of the same reactions because of the fast isomerization of propyne and allene. Thus the modeling results satisfactorily explain the nearly identical ignition characteristics for both fuels observed experimentally [67].

Laminar Flame Speeds and Ignition Delay of Propane

The present kinetic model was also tested against the atmospheric propane flame speed data of Vagelopoulos et al. [68]. Figure 18 presents a comparison between the computationally and experimentally determined propane flame speeds. With the current propene, propyne, and allene submechanism, the kinetics relevant to propane oxidation suggested by Tsang [45] predict the shape and magnitude of the flame speed data very well. Based on the model, propane consumption in near-stoichiometric flames is predominately by the H abstraction by the H-atom forming the two propyl radicals $n$$C_3H_7$ and $i$$C_3H_7$,

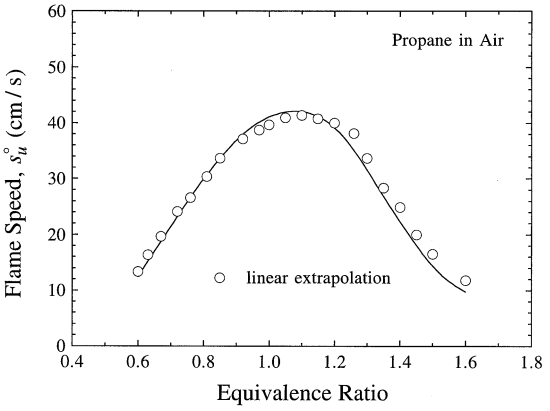

Fig. 18. Comparison of experimental (symbols, [68]) and computed (line) laminar flame speeds of propane/air mixtures at 1 atm.

$$C_3H_8 + H = nC_3H_7 + H_2 \qquad \text{(R111)}$$

$$C_3H_8 + H = iC_3H_7 + H_2. \qquad \text{(R112)}$$

The radicals quickly decompose via

$$nC_3H_7 = C_2H_4 + CH_3 \qquad (-\text{R90})$$

$$iC_3H_7 = C_3H_6 + H, \qquad (-\text{R99})$$

forming propene and ethylene. A sensitivity analysis was also conducted to determine which reactions are influential to flame speed prediction. For most conditions the most influential reactions were found to be those of hydrogen and C_1 hydrocarbon species. For very fuel-rich conditions with ϕ = 1.4, however, the H-abstraction reactions of C_3H_6 and C_3H_8 by the H-atom become somewhat influential.

Comparisons were also made between the predicted and experimentally determined ignition delay data of Burcat et al. [69], as shown in Fig. 19. The numerical results were obtained

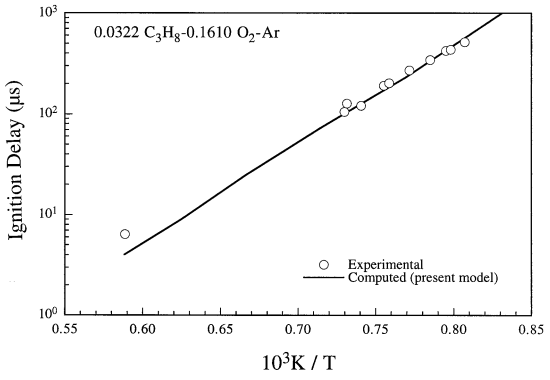

Fig. 19. Experimental (symbols, [69]) and computed (lines) ignition delay times for a 3.22% propane, 16.1% oxygen, and 80.68% argon mixture at temperatures ranging from 1240–1690 K and pressures ranging from 7.8 to 15.4 atm. Calculations were made with an average molar density of 9.4×10^{-5} mol/cm^3.

between the temperatures of 1200–1700 K and at an average molar density of 9.39×10^{-5} mol/cm^3. It is seen that the model predicts fairly well the ignition delay times for propane mixtures, throughout the entire temperature range. Based on the model, the most influential reaction on ignition delay is $H + O_2 = O + OH$, followed by $CH_3 + HO_2 = CH_3O + OH$, the propane unimolecular dissociation via the reverse of (R110),

$$C_2H_5 + CH_3(+M) = C_3H_8(+M), \qquad \text{(R110)}$$

and H-abstraction of C_3H_8 by the H-atom (R111).

SUMMARY

Propene pyrolysis and oxidation were experimentally studied in the PTFR at ~1200 K and atmospheric pressure. In addition, the laminar flame speeds of propene in air were determined over the equivalence ratio range of 0.7 to 1.7 and at atmospheric pressure. A detailed kinetic model was compiled, largely based on the GRI-Mech, the compilations of Tsang, and our previous studies for the key reactions of propyne and allene oxidation and pyrolysis. It was shown that the detailed kinetic model could reconcile a significant body of combustion data for propene, propyne, allene, and propane. These data include propene and propyne pyrolysis and oxidation in the PTFR and in flames, propyne and allene ignition in shock tubes, and propane oxidation in flames and shock tubes.

Significant uncertainties still remain and are identified as the high-temperature reaction kinetics of propene unimolecular decomposition reactions, and the recombination of propargyl. Despite the ample agreement achieved by the kinetic model proposed herein over a wide range of conditions, resolving these uncertainties is imperative for further achieving fundamental and quantitative predictions of the combustion of C_3H_x and higher hydrocarbon fuels.

The authors thank Mr. Joe Sivo and Stephen Zeppieri for their generous help in the PTFR experiment and Professors Irvin Glassman and Frederick Dryer for making the PTFR facility accessible to us. The work was supported by the New World Vista Program of the Air Force Office of Scientific Research under the technical monitoring of Dr. Julian M. Tishkoff.

REFERENCES

1. Westbrook, C. K., and Dryer, F. L., *Prog. Energy Combust. Sci*. 10:1–57 (1984).
2. Leung, K. M., and Lindstedt, R. P., *Combust. Flame* 102:129–160 (1995).
3. Davis, S. G., and Law, C. K., *Twenty-Seventh Symposium (International) on Combustion*, The Combustion Institute, Pittsburgh, 1998, p. 521.
4. Alkemade, U., and Homann, K. H., *Z. Physik. Chem. Neue Folge* 161:19–34 (1989).
5. Stein, S. E., Walker, J. A., Suryan, M. M., and Fahr, A., *Twenty-Third Symposium (International) on Combustion*, The Combustion Institute, Pittsburgh, 1991, p. 85.
6. Miller, J. A., and Melius, C. F., *Combust. Flame* 91:21–39 (1992).
7. Gibbs, G. J., and Calcote, H. F., *J. Chem. Eng. Data* 4:226–237 (1959).
8. Gerstein, M., Levine, O., and Wong, E. L., *J. Am. Chem. Soc*. 73:418–422 (1951).
9. Günther, R., and Janisch, G., *Chemie Ing. Techn*. 43:975–978 (1971).
10. Burcat, A., and Radhakrishnan, K., *Combust. Flame* 60:157–169 (1985).
11. Westbrook, C. K., and Pitz, W. J., *Combust. Sci. Technol*. 37:117–152 (1984).
12. Dagaut, P., Cathonnet, M., and Boettner, J. C., *J. Phys. Chem*. 92:661–671 (1988).
13. Dagaut, P., Cathonnet, M., and Boettner, J. C., *Combust. Sci. Technol*. 83:167–185 (1992).
14. Thomas, S. D. (1992). Ph.D. dissertation, Chemical

Engineering Department, University of Massachusetts, Amherst.
15. Thomas, S. D., Bhargava, A., Westmoreland, P. R., Lindstedt, R. P., and Skevis, G., *Bull. Soc. Chim. Belg*. 105:501–512 (1996).
16. Wilk, R. D., Cernansky, N. P., Pitz, W. J., and Westbrook, C. K., *Combust. Flame* 77:145–170 (1989).
17. Stark, M. S., and Waddington, D. J., *Int. J. Chem. Kinet*. 27:123–151 (1995).
18. Chappell, G. A., and Shaw, H., *J. Phys. Chem*. 72:4672–4675 (1968).
19. Burcat, A., *Fuel* 54:87–93 (1975).
20. Kiefer, J. H., Al-Alami, M. Z., and Budach, K. A., *J. Phys. Chem*. 86:808–813 (1982).
21. Rao, V. S., and Skinner, G. B., *J. Phys. Chem*. 93:1869–1876 (1989).
22. Hidaka, Y., Nakamura, T., Tanaka, H., Jinno, A., Kawano, H., and Higashihara, T., *Int. J. Chem. Kinet*. 24:761–780 (1992).
23. Davis, S. G., Law, C. K., and Wang, H., *Twenty-Seventh Symposium (International) on Combustion*, The Combustion Institute, Pittsburgh, 1998, p. 305.
24. Davis, S. G., Law, C. K., and Wang, H., Propyne pyrolysis in a flow reactor: an experimental, RRKM, and detailed kinetic modeling study, *J. Phys. Chem*., in press.
25. Law, C. K., *Twenty-Second Symposium (International) on Combustion*, The Combustion Institute, Pittsburgh, 1988, p. 1381.
26. Wu, C. K., and Law, C. K., *Twentieth Symposium (International) on Combustion*, The Combustion Institute, Pittsburgh, 1984, p. 1941.
27. Davis, S. G., Wang, H., Brezinsky, K., and Law, C. K., *Twenty-Sixth Symposium (International) on Combustion*, The Combustion Institute, Pittsburgh, 1996, p. 1025.
28. Brezinsky, K., Litzinger, T. A., and Glassman, I., *Int. J. Chem. Kinet*. 16:1053–1074 (1984).
29. Frenklach, M., Wang, H., Goldenberg, M., Smith, G. P., Golden, D. M., Bowman, C. T., Hanson, R. K., Gardiner, W. C., and Lissianski, V. (1995). *GRI-Mech—An Optimized Detailed Chemical Reaction Mechanism for Methane Combustion*. GRI Technical Report No. GRI-95/0058.
30. Wang, H., Hahn, T. O., Sung, C. J., and Law, C. K., *Combust. Flame* 105:291–307 (1996).
31. Sun, C. J., Sung, C. J., Wang, H., and Law, C. K., *Combust. Flame* 107:321–335 (1996).
32. Wang, H., and Frenklach, M., *Combust. Flame* 110: 173–221 (1997).
33. Tsang, W., *J. Phys. Chem. Ref. Data* 20:221–273 (1991).
34. Gilbert, R. G., Luther, K., and Troe, J., *Ber. Bunsenges. Phys. Chem*. 87:169–177 (1983).
35. Tsang, W., and Hampson, R. F., *J. Phys. Chem. Ref. Data* 15:1087–1279 (1986).
36. Bozzelli, J. W., and Dean, A. M., *J. Phys. Chem*. 97:4427–4441 (1993).
37. Baulch, D. L., Cobos, C. J., Cox, R. A., Frank, P., Hayman, G., Just, T. H., Kerr, J. A., Murrells, T., Pilling, M. J., Troe, J., Walker, R. W., and Warnatz, J., *J. Phys. Chem. Ref. Data* 21:411–736 (1992).
38. Adusei, G. Y., Blue, A. S., and Fontijn, A., *J. Phys. Chem*. 100:16921–16924 (1996).
39. Wu, C. H., and Kern, R. D., *J. Phys. Chem*. 91:6291–6296 (1987).
40. Pauwels, J-F., Volponi, J. V., and Miller, J. A., *Combust. Sci. Technol*., 110–111:249–276 (1995).
41. Miller, J. A., and Bowman, C. T., *Prog. Energy Combust. Sci*. 15:287–338 (1989).
42. Slagle, I. R., and Gutman, D., *Twenty-First Symposium (International) on Combustion*, The Combustion Institute, Pittsburgh, 1986, p. 875.
43. Warnatz, J., Bockhorn, H., Möser, A., and Wenz, H. W., *Nineteenth Symposium (International) on Combustion*, The Combustion Institute, Pittsburgh, 1983, p. 197.
44. Kerr, J. A., and Parsonage, M. J., *Evaluated Kinetic Data on Gas Phase Addition Reactions: Reactions of Atoms and Radicals with Alkenes, Alkynes and Aromatic Compounds*, Butterworths, London, 1972.
45. Tsang, W., *J. Phys. Chem. Ref. Data*, 17:887–951 (1988).
46. Ko, T., Adusei, G. Y., and Fontijn, A., *J. Phys. Chem*. 95:9366–9370 (1991).
47. Adusei, G. Y., and Fontijn, A., *J. Phys. Chem*. 97:1406–1408 (1993).
48. Wang, H., and Frenklach, M., *J. Phys. Chem*. 98:11465–11489 (1994).
49. Gutman, D., Slagle, A., Bencsura, A., and Xing, S.-B., *ACS Preprints*, *Div. Fuel Chem*. 36:1509–1517 (1991).
50. Slagle, I. R., Bernhardt, J. R., and Gutman, D., *Twenty-Second Symposium (International) on Combustion*, The Combustion Institute, Pittsburgh, 1989, p. 953.
51. Homann, K. J., and Wellmann, C., *Ber. Bunsenges. Phys. Chem*. 87:527–533 (1983).
52. Perry, R. A., *Combust. Flame* 58:221–227 (1984).
53. Kiefer, J. H., Mizerka, L. J., Patel, M. R., and Wei, H.-C., *J. Phys. Chem*. 89:2013–2019 (1985).
54. Frank, P., Herzler, J., Just, T., and Wahl, C., *Twenty-Fifth Symposium (International) on Combustion*, The Combustion Institute, Pittsburgh, 1994, p. 833.
55. He, Y. Z., Mallard, W. G., and Tsang, W., *J. Phys. Chem*. 92:2196–2201 (1988).
56. Emdee, J. L., Brezinsky, K., and Glassman, I., *J. Phys. Chem*. 96:2151–2161 (1992).
57. Marinov, N. M., Pitz, W. J., Westbrook, C. K., Castaldi, M. J., and Senkan, S. M., *Combust. Sci. Technol*. 116:211–287 (1996).
58. Böhland, T., Temps, F., and Wagner, H. G., *Twenty-First Symposium (International) on Combustion*, The Combustion Institute, Pittsburgh, 1986, p. 841.
59. Kiefer, J. H., Mudipalli, P. S., Sidhu, S. S., Kern, R. D., Jursic, B. S., Xie, K., and Chen, H., *J. Phys. Chem. A* 101:4057 (1997).
60. Burcat, A., and McBride, B., (1997). *1997 Ideal Gas Thermodynamic Data for Combustion and Air-Pollution Use*. Technion Aerospace Engineering (TAE) Rept. No. 804.
61. Tsang, W., in *Heats of Formation of Organic Free Radicals by Kinetic Methods in Energetics of Organic*

Free Radicals (J. A. Martinho Simoes, A. Greenberg, and J. F. Liebman, Eds.), Blackie Academic and Professional, London, 1996, p. 22.
62. Kee, R. J., Rupley, F. M., and Miller, J. A. (1989). Sandia Report SAND 89-8009B, Sandia National Laboratories, Albuquerque, NM.
63. Kee, R. J., Grcar, J. F., Smooke, M. D., and Miller, J. A. (1985). Sandia Report SAND85-8240 UC4, Sandia National Laboratories, Albuquerque, NM.
64. Lutz, A. E., Kee, R. J., Miller, J. A. (1988). Sandia Report SAND87-8248, Sandia National Laboratories, Albuquerque, NM.
65. Held, T. J., Marchese, A. J., and Dryer, F. L., *Combust. Sci. Technol*. 123:107–146 (1997).
66. Miller, J. A., *Twenty-Sixth Symposium (International) on Combustion*, The Combustion Institute, Pittsburgh, 1996, p. 461.
67. Curran, H., Simmie, J. M., Dagaut, P., Voisin, D., Cathonnet, M., *Twenty-Sixth Symposium (International) on Combustion*, The Combustion Institute, Pittsburgh, 1996, p. 613.
68. Vagelopoulos, C. M., Egolfopoulos, F. N., and Law, C. K., *Twenty-Fifth Symposium (International) on Combustion*, The Combustion Institute, Pittsburgh, 1994, p. 1341.
69. Burcat, A., Scheller, K., and Lifshitz, A., *Combust. Flame* 16:29–33 (1971).

Received 29 July 1998; revised 27 April 1999; accepted 6 May 1999